

# Optical spectroscopy and X-ray detections of a sample of quasars and AGN selected in the mid-infrared from two *Spitzer* wide-area surveys.

M. Lacy<sup>1</sup>, A. Petric<sup>1,3</sup>, A. Sajina<sup>1</sup>, G. Canalizo<sup>2</sup>, L.J. Storrie-Lombardi<sup>1</sup>, L. Armus<sup>1</sup>, D. Fadda<sup>1</sup>, F.R. Marleau<sup>1</sup>

## ABSTRACT

We present optical spectroscopy of a sample of 77 luminous AGN and quasars selected on the basis of their mid-infrared colors. Our objects are selected from the *Spitzer* Extragalactic First Look Survey and SWIRE XMM-LSS fields, with a typical  $24\mu\text{m}$  flux density of  $5\text{mJy}$ . The median redshift is 0.6, with a range of  $\sim 0.05 - 4$ . Only 33% (25/77) of these objects are normal type-1 quasars, with no obscuration. 44% (34/77) are type-2 objects, with high-ionization, narrow emission lines, 14% (11/77) are dust-reddened type-1 quasars, showing broad lines but a dust-reddened or unusually weak quasar continuum. 9% (7/77) show no sign of an AGN in the optical spectrum, having either starburst spectra or spectra which could be of either starburst or LINER types. These latter objects are analogous to the X-ray detected population of AGN with weak or non-existent optical AGN emission (the “XBONGs”). 21 of our objects from the SWIRE field fall within moderately-deep XMM exposures. All the unobscured quasars, and about half the obscured quasars are detected in these exposures. This sample, when taken together with other samples of *Spitzer* selected AGN and quasars, and results from X-ray studies, confirms that obscured AGN dominate the AGN and quasar number counts of all rapidly-accreting supermassive black hole systems, at least for  $z \lesssim 4$ . This implies a high radiative efficiency for the black hole accretion process.

*Subject headings:* quasars:general – galaxies:Seyfert – infrared:galaxies

## 1. Introduction

Quasars whose optical emission is hidden by dust in the optical and gas in the soft X-ray have always been hard to find. However, a large type-2 (hidden) quasar population has long been predicted, both from the statistics of Seyfert-1 and 2 galaxies, and from those of radio galaxies and radio-loud quasars. A large population of hidden AGN is also predicted from models of the X-ray background (e.g. Comastri et al. 1995; Worsley et al. 2005), though most models predict these

AGN to be of Seyfert rather than quasar luminosity. Some success in finding dust obscured quasars has been obtained using selection based on the Two Micron All Sky Survey (2MASS) to find lightly dust-reddened (rest frame extinctions  $A_V \sim 2$ ) quasars, based either on 2MASS colors alone (Cutri et al. 2001), or on 2MASS combined with a radio detection and very red optical-IR colors (Glikman et al. 2005). Only recently, however, have large samples of type-2 quasars, with rest-frame  $A_V \gtrsim 5$  been found. Zakamska et al. (2003) used the Sloan Digital Sky Survey (SDSS) to find objects with the high-ionization narrow-line spectra characteristic of type-2 AGN. Combining *ISO* and 2MASS data allowed Haas et al. (2004a) and Leipski et al. (2005) to find significant numbers of obscured AGN, including several type-2 quasars. *Spitzer* data has been used

<sup>1</sup>Spitzer Science Center, Caltech,  
Mail Code 220-6, Pasadena, CA 91125;  
mlacy@ipac.caltech.edu, sajina@ipac.caltech.edu,  
lisa@ipac.caltech.edu

<sup>2</sup>University of California, Riverside

<sup>3</sup>Columbia University of New York

to find highly-obscured AGN, both through mid-infrared color selection (Lacy et al. 2004 [hereafter Paper I], 2005a; Stern et al. 2005; Alonso-Herrero et al. 2005; Polletta et al. 2006) and joint radio-infrared selection (Martínez-Sansigre et al. 2005, 2006; Weedman et al. 2006; Donley et al. 2005). Type-1 quasars selected through joint Spitzer and optical colors and/or morphologies have been targeted by several groups (Brown et al. 2005; Hatziminaoglou et al. 2005; Siana et al. 2006). Also, the mid-infrared properties of X-ray selected AGN have been discussed by Treister et al. (2005) and Barmby et al. (2005).

Mid-infrared selection of AGN is effective because dust heated by the AGN forms a “calorimeter”, whose luminosity is not as strongly affected by obscuration as that in most other wavelength bands (except the radio) (e.g. Spinoglio et al. 1995; Meisenheimer et al. 2001; Ogle et al. 2006). Richards et al. (2006) show that the bolometric correction in the mid-infrared varies little for different subsamples of type-1 quasars (e.g. optically or infrared luminous, optically-red or optically blue), or luminosity, and that about 15% of the bolometric luminosity of a quasar is emitted at mid-infrared wavelengths. Integration over the Richards et al. (2006) mean quasar SED as a whole suggests that about 40% of the emission from a typical quasar is reprocessed by dust in the infrared. This means that mid-infrared selection of AGN is probably a good proxy for selection on the basis of bolometric luminosity, at least for those objects which are not so highly obscured that their mid-infrared luminosity is significantly suppressed. Much of the dust emission is thought to arise in the “obscuring torus” required by Unified Schemes (e.g. Antonucci 1993), though it is becoming increasingly clear that host dust in the narrow line region of AGN also contributes significantly (e.g. Mason et al. 2006). AGN are an important global contributor to the mid-infrared luminosity density. Brand et al. (2006) show that the luminosity density of mid-IR emission in samples of MIPS  $24\mu\text{m}$  sources selected at mJy levels is dominated by AGN, only at submJy levels do star forming galaxies begin to dominate.

In this paper, we focus on optical spectroscopic follow-up of AGN candidates selected according to the mid-infrared color criteria presented in Paper I. By selecting relatively bright objects from

wide-area *Spitzer* surveys we are able to find many obscured AGN with mid-infrared luminosities typical of quasars at moderate redshifts. These objects provide a good complement to the mostly lower-luminosity or higher redshift AGN found in surveys such as the Great Observatories Origins Deep Survey (GOODS) and the Chandra Deep fields. Preliminary results from the spectroscopic follow-up of the sample presented in Paper 1 were given in Lacy et al. (2005a). In this paper, we describe the selection of samples of mid-infrared selected AGN candidates flux-limited at  $24\mu\text{m}$  from both the Extragalactic First Look Survey (XFLS) and the *Spitzer* Wide-area Infrared Extragalactic Survey (SWIRE) XMM-LSS field (Lonsdale et al. 2005), and their spectroscopic follow-up observations. We classify the optical spectra according to the type of AGN, and use them to place a lower bound on the fraction of obscured quasars and luminous Seyfert galaxies. We also investigate the X-ray fluxes of those objects which fall on archival observations made with the X-ray Multiple Mirror telescope (*XMM-Newton*). A more detailed analysis of the Spectral Energy Distributions (SEDs) and X-ray properties of the AGN will be carried out in a later paper (Petric et al. 2006).

We assume a cosmology with  $\Omega_M = 0.3$ ,  $\Omega_\Lambda = 0.7$  and  $H_0 = 70\text{kms}^{-1}\text{Mpc}^{-1}$ .

## 2. The Spitzer XFLS and SWIRE AGN samples

We selected samples of AGN by mid-infrared color from the XFLS and SWIRE XMM fields. The basis of our color selection technique is described in Sajina, Lacy & Scott (2005) and Paper I, though the samples in this paper are flux-limited at  $24\mu\text{m}$  rather than at  $8\mu\text{m}$  as was the case for the sample of Paper 1. To obtain the XFLS sample, we began by matching the XFLS  $24\mu\text{m}$  catalog of Fadda et al. (2006) to the Infrared Array Camera (IRAC) 4-band catalog of Lacy et al. (2005). All MIPS  $24\mu\text{m}$  detections with detections in all four IRAC bands were then plotted on the color-color diagram of Figure 1. For the SWIRE XMM sample, we used the band-merged SWIRE IRAC/MIPS  $24\mu\text{m}$  catalog available from the *Spitzer* popular products website. The color cut used to select AGN candidates was  $\lg(S_{5.8}/S_{3.6}) > -0.1$  and  $\lg(S_{8.0}/S_{4.5}) > -0.2$

and  $\lg(S_{8.0}/S_{4.5}) \leq 0.8\lg(S_{5.8}/S_{3.6}) + 0.5$ . The  $\lg(S_{5.8}/S_{3.6})$  cut was moved by +0.1 compared to Paper I. The exact position of this cut is not critical, and it was felt that shifting this would help remove non-AGN contaminants, particularly as the final  $5.8\mu\text{m}$  fluxes in the XFLS catalogue were increased by  $\approx 10\%$  in the final version of the XFLS catalog relative to the catalog used in Paper I. We discuss the exact placement of the color cuts with respect to the completeness of the AGN selection in section 5.3. Candidates were selected down to limiting  $24\mu\text{m}$  fluxes of 4.4mJy in the XFLS and 6.6mJy in the SWIRE XMM field.

The  $24\mu\text{m}$  flux limited sample should be an improvement on  $8\mu\text{m}$  selection by making us more sensitive to highly-reddened objects, and high redshift objects, where the strong  $k$ -correction on the mid-infrared dust emission means that they drop out of flux-limited samples selected at shorter wavelengths. The disadvantage of this selection is that we will be missing objects at  $z \sim 1.5$  which have strong silicate absorption in the  $24\mu\text{m}$  band, however, as our median redshift is  $\approx 0.6$  only a few objects will be missed due to this effect. The XFLS sample is complete for objects falling in the IRAC ‘‘AGN wedge’’ color selection to a flux limit of 4.6mJy at  $24\mu\text{m}$ , and the SWIRE sample to a flux limit of 6.6mJy (note that all MIPS sources down to these flux limits have 4-band IRAC detections). Approximately 20% of MIPS  $24\mu\text{m}$  sources at these flux levels fall into our AGN-dominated part of the color-color plot.

A few stars and nearby galaxies have been removed from the samples. Most stars were only present in the initial selection due to photometric errors related to saturation in the shorter IRAC bands, though one star (SSTXFLS J172432.8+592646, see Paper I) has the correct colors to fall in the sample, presumably due to a dust disk. Very low redshift ( $z \lesssim 0.05$ ) galaxies are also possible contaminants due to the presence of  $6.2\mu\text{m}$  PAH emission in the  $5.8\mu\text{m}$  band of IRAC (Sajina, Lacy & Scott 2005). The interacting galaxy Arp 54 appeared in the selection of the SWIRE AGN sample, but has been removed for this reason.

Tables 1 and 2 contain the observing logs for our samples. Most data were taken with the Cosmic instrument on the Palomar 200-inch. Some spectra were obtained with the ISIS instrument at the 4.2m William Herschel Telescope (WHT)

on La Palma, with ESI at the Keck II telescope, or with the Kast spectrograph at the 3m Shane Telescope at Lick Observatory. SSTXFLS J172248.9+583256, for which we failed to obtain a redshift in the optical was observed in the near-infrared using the low dispersion mode of the Spex instrument at the Infrared Telescope Facility (IRTF) (Rayner et al. 2003). Data were analysed in IRAF using standard routines for flat fielding, wavelength calibration and sky subtraction. No attempt has been made to correct for reddening. An extinction correction has been applied based on airmass, but no attempt has been made to correct the telluric absorption features. The spectra are approximately photometrically calibrated, but variable seeing and cirrus cloud means that we expect our spectrophotometric accuracy to be no better than 50%. In the XFLS field, most quasars have spectra from the Sloan Digital Sky Survey (SDSS), which have been used where they exist. A few of the quasars in the SWIRE field have redshifts from the literature. Several of our XFLS sources have spectra in the Multiple Mirror Telescope (MMT) spectroscopic survey of Papovich et al (2006; hereafter P06), including one object missed from our original selection but which is within the flux-limited sample (SSTXFLS J171454.4+584948). The spectra of all the objects with the exception of the SWIRE quasars with redshifts from the literature are shown in Figures 2 and 3. Objects with spectral classifications from both this paper and Papovich et al. (2006) are discussed in Appendix A. For completeness, Appendix B contains details of the results of spectroscopy on the objects in the  $8\mu\text{m}$  sample of Paper I which are too faint at  $24\mu\text{m}$  to fall in the XFLS sample.

### 3. Results

#### 3.1. Optical spectral classification of the AGN candidates

We have used a combination of standard classification schemes to classify our AGN candidates, principally because the large redshift and luminosity range of our sample makes any single scheme unworkable. We divide our objects into four main classes. Normal quasars/Seyfert-1 galaxies are assigned type 1. The obscured quasars are subdivided into three classes. Reddened quasars, show-

Table 1: Observing log for the XFLS AGN sample

Name	Date observed	Telescope/Instrument	Exposure	Slit	Airmass	PA
SSTXFLS J171115.2+594906	2004 August 19	Palomar 200/DbleSpec	2 × 600	2.0	1.32	105
SSTXFLS J171147.4+585839	2004 August 18	Palomar 200/DbleSpec	2 × 600	2.0	1.44	95
SSTXFLS J171233.4+583610	2005 Oct 30	Palomar 200/Cosmic	2×900	2.0	1.40	90
SSTXFLS J171302.3+593610	2005 June 01	Palomar 200/Cosmic	2× 1200	1.5	1.15	0
SSTXFLS J171313.9+603146	2004 July 18	Keck II/ESI	1×600	1.0	1.55	127
SSTXLFS J171324.2+585549	2004 August 19	Palomar 200/DbleSpec	2 × 600	2.0	1.35	100
SSTXFLS J171325.1+590531	2005 Nov 01	Palomar 200/Cosmic	1× 900	1.5	1×90076	
SSTXFLS J171331.5+585804	2005 June 02	Palomar 200/Cosmic	2×1200	1.5	1.15	165
SSTXFLS J171335.1+584756	2005 June 01	Palomar 200/Cosmic	2×600	1.5		90
SSTXFLS J171345.5+600730	2005 Oct 30	Palomar 200/Cosmic	2×1800	2.0	1.70	90
SSTXFLS J171345.5+600730	2006 June 27	Palomar 200/Cosmic	3×1800	2.0	1.13	180
SSTXFLS J171419.9+602724	2005 June 02	Palomar 200/Cosmic	1×1200	1.5	1.18	45
SSTXFLS J171430.7+584225	2005 Oct 31	Palomar 200/Cosmic	2×900	1.5	1.86	190
SSTXLFS J171513.8+594638	2002 June 15	Shane/Kast	1× 1200	1.5	1.24	73
SSTXFLS J171530.7+600216	2005 June 01	Palomar 200/Cosmic	1×600	1.5	1.15	140
S						
SSTXFLS J171650.6+595752	2005 June 02	Palomar 200/Cosmic	1×600	1.5	1.23	110
SSTXFLS J171708.6+591341	2005 June 02	Palomar 200/Cosmic	1×900	1.5	1.26	110
SSTXFLS J171750.7+584745	2005 Oct 30	Palomar 200/Cosmic	2×1800	2.0	1.50	90
SSTXFLS J171754.6+600913	2005 June 01	Palomar 200/Cosmic	2× 1200	1.5	1.12	0
SSTXFLS J171831.5+595317	2004 July 13	WHT/ISIS	2×600	2.0	1.19	5
SSTXFLS J171839.6+593359	2002 June 11	Shane/Kast	1× 1200	1.5	1.26	109
SSTXFLS J171913.5+584508	2005 June 01	Palomar 200/Cosmic	2×600	1.5	1.18	140
SSTXFLS J172044.8+582923	2005 June 02	Palomar 200/Cosmic	2×1800	2.0	1.11	90
SSTXFLS J172050.4+591511	2004 July 13	WHT/ISIS	2×900	2.0	1.16	85
SSTXFLS J172050.4+591511	2006 June 28	Palomar 200/Cosmic	3×1800	1.5	1.15	210
SSTXFLS J172123.1+601214	2004 July 18	Keck II/ESI	1×600	1.0	1.57	125
SSTXFLS J172219.5+594506	2005 June 02	Palomar 200/Cosmic	2×600	1.5	1.48	90
SSTXFLS J172228.1+601526	2005 June 02	Palomar 200/Cosmic	1×1200	1.5	1.24	45
SSTXFLS J172245.0+590328	2005 Nov 01	Palomar 200/Cosmic	2×1200	1.5	1.55	100
SSTXFLS J172248.9+583256	2005 June 02	Palomar 200/Cosmic	2×1200	1.5	1.12	45
SSTXFLS J172248.9+583256	2006 May 26	IRTF/Spex	22×120	0.5	1.48	100
SSTXFLS J172328.4+592947	2004 August 19	Palomar 200/DbleSpec	2 × 600	2.0	1.5	90
SSTXFLS J172542.3+595317	2005 June 02	Palomar 200/Cosmic	2× 1200	1.5	1.34	90

Table 2: Observing log for the SWIRE XMM-LSS sample

Name	Date observed	Telescope/Instrument	Exposure	Slit	Airmass	PA
SWIRE2 J021638.21-042250.8	2005 Oct 30	Palomar 200/Cosmic	1× 900	1.5	1.45	125
SWIRE2 J021657.77-032459.7	2005 Oct 29	Palomar 200/Cosmic	1× 600	1.5	1.84	225
SWIRE2 J021729.06-041937.8	2005 Oct 30	Palomar 200/Cosmic	2×1800	1.5	1.4	20
SWIRE2 J021749.00-052306.9	2005 Nov 01	Palomar 200/Cosmic	2×1800	1.5	1.30	7
SWIRE2 J021759.91-052056.1	2005 Oct 31	Palomar 200/Cosmic	2×1200	1.5	1.28	20
SWIRE2 J021809.45-045945.9	2005 Oct 31	Palomar 200/Cosmic	2×1200	1.5	1.31	20
SWIRE2 J021859.74-040237.2	2005 Oct 30	Palomar 200/Cosmic	1× 600	1.5	1.89	312
SWIRE2 J021909.60-052512.9	2005 Oct 29	Palomar 200/Cosmic	1× 600	1.5	1.31	150
SWIRE2 J021938.70-032508.2	2005 Nov 01	Palomar 200/Cosmic	1×600	1.5	1.40	42
SWIRE2 J021939.08-051133.8	2005 Oct 29	Palomar 200/Cosmic	1× 600	1.5	1.36	90
SWIRE2 J022005.93-031545.7	2005 Nov 01	Palomar 200/Cosmic	1×600	1.5	1.55	47
SWIRE2 J022012.21-034111.8	2005 Nov 01	Palomar 200/Cosmic	1×600	1.5	1.74	47
SWIRE2 J022039.48-030820.3	2005 Oct 31	Palomar 200/Cosmic	1× 900	1.5	1.50	140
SWIRE2 J022133.82-054842.8	2005 Nov 01	Palomar 200/Cosmic	1×600	1.5	1.75	145
SWIRE2 J022211.57-051308.1	2005 Nov 01	Palomar 200/Cosmic	2×1800	1.5	1.31	341
SWIRE2 J022225.86-050015.1	2005 Oct 31	Palomar 200/Cosmic	1×600	1.5	2.24	48
SWIRE2 J022255.87-051351.7	2005 Oct 31	Palomar 200/Cosmic	1×900	1.5	1.49	30
SWIRE2 J022301.97-052335.8	2005 Nov 01	Palomar 200/Cosmic	2×1200	1.5	1.46	341
SWIRE2 J022306.74-050529.1	2005 Oct 30	Palomar 200/Cosmic	2× 900	1.5	1.76	315
SWIRE2 J022310.42-055102.7	2005 Oct 29	Palomar 200/Cosmic	2× 1800	2.0	1.24	90
SWIRE2 J022348.96-025426.0	2005 Nov 01	Palomar 200/Cosmic	1×900	1.5	1.47	145
SWIRE2 J022356.49-025431.1	2005 Oct 29	Palomar 200/Cosmic	2×1800	2.0	1.24	90
SWIRE2 J022422.27-031054.7	2005 Oct 31	Palomar 200/Cosmic	1×600	1.5	1.67	48
SWIRE2 J022431.58-052818.8	2005 Oct 31	Palomar 200/Cosmic	1× 600	1.5	1.7	310
SWIRE2 J022438.97-042706.3	2005 Nov 01	Palomar 200/Cosmic	1×600	1.5	1.95	45
SWIRE2 J022455.77-031153.6	2005 Oct 31	Palomar 200/Cosmic	1×900	1.5	1.52	40
SWIRE2 J022508.33-053917.7	2005 Oct 31	Palomar 200/Cosmic	1× 900	1.5	1.32	26
SWIRE2 J022542.02-042441.1	2005 Oct 30	Palomar 200/Cosmic	2× 900	1.5	1.6	40
SWIRE2 J022600.01-035954.5	2005 Oct 31	Palomar 200/Cosmic	1× 900	1.5	1.45	125
SWIRE2 J022612.67-040319.4	2005 Oct 31	Palomar 200/Cosmic	1×600	1.5	1.88	48
SWIRE2 J022700.77-042020.6	2005 Oct 29	Palomar 200/Cosmic	1× 600	1.5	1.32	150

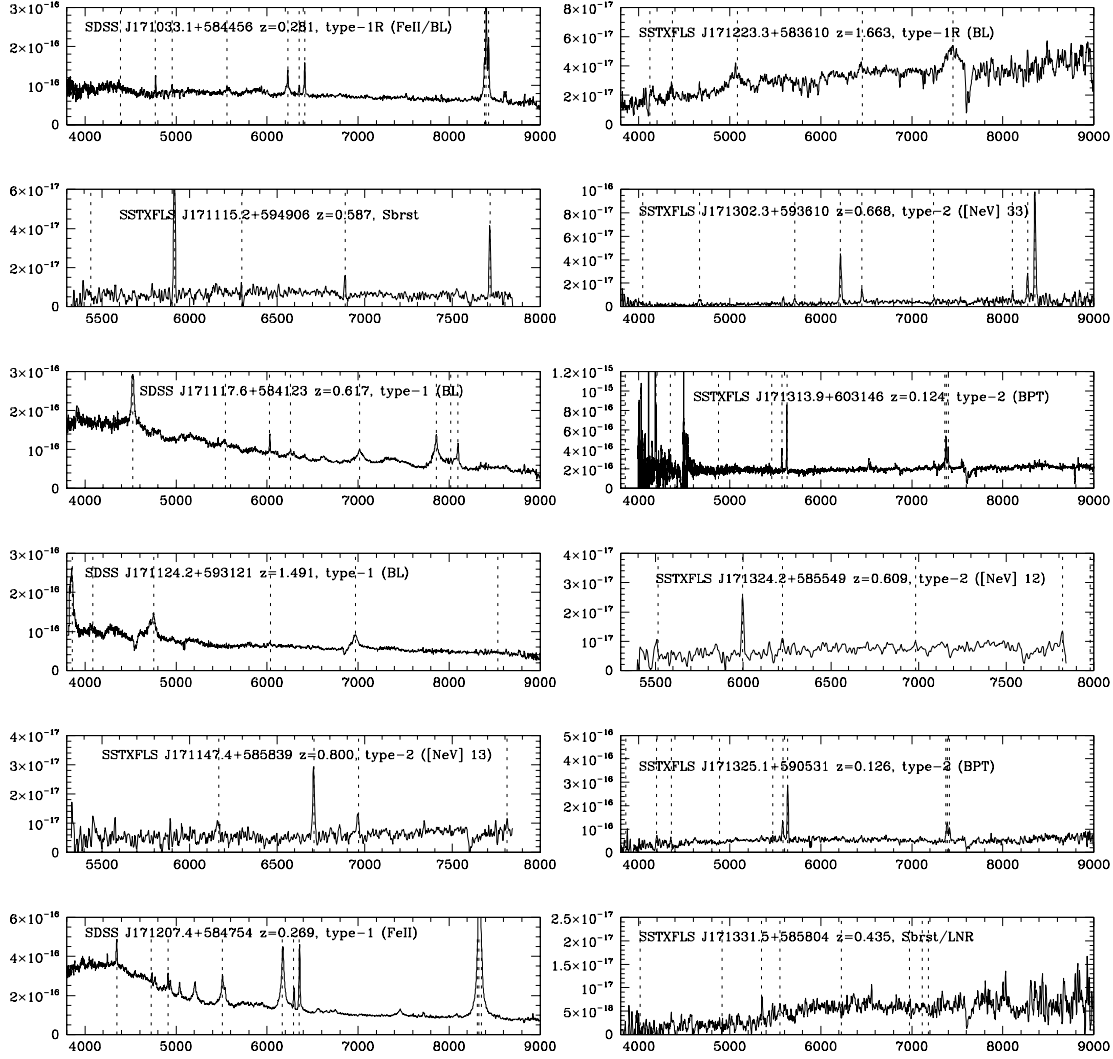


Fig. 2.— Optical spectra of the XFLS AGN candidates. Dotted lines indicate the positions of redshifted emission lines (not all of which are necessarily detected in a given spectrum). The emission lines indicated are (from blue to red): Ly $\alpha$ , Nv1240, Civ 1549, HeII1640, CIII]1909, [NeV]2424, MgII2798, [NeV]3426, [OIII]3727, [NeIII]3869, H $\gamma$ , H $\beta$ , [OIII]4959, [OIII]5007, [NII]6548, H $\alpha$  and [NII]6584. The spectra are presented in order of Right Ascension.

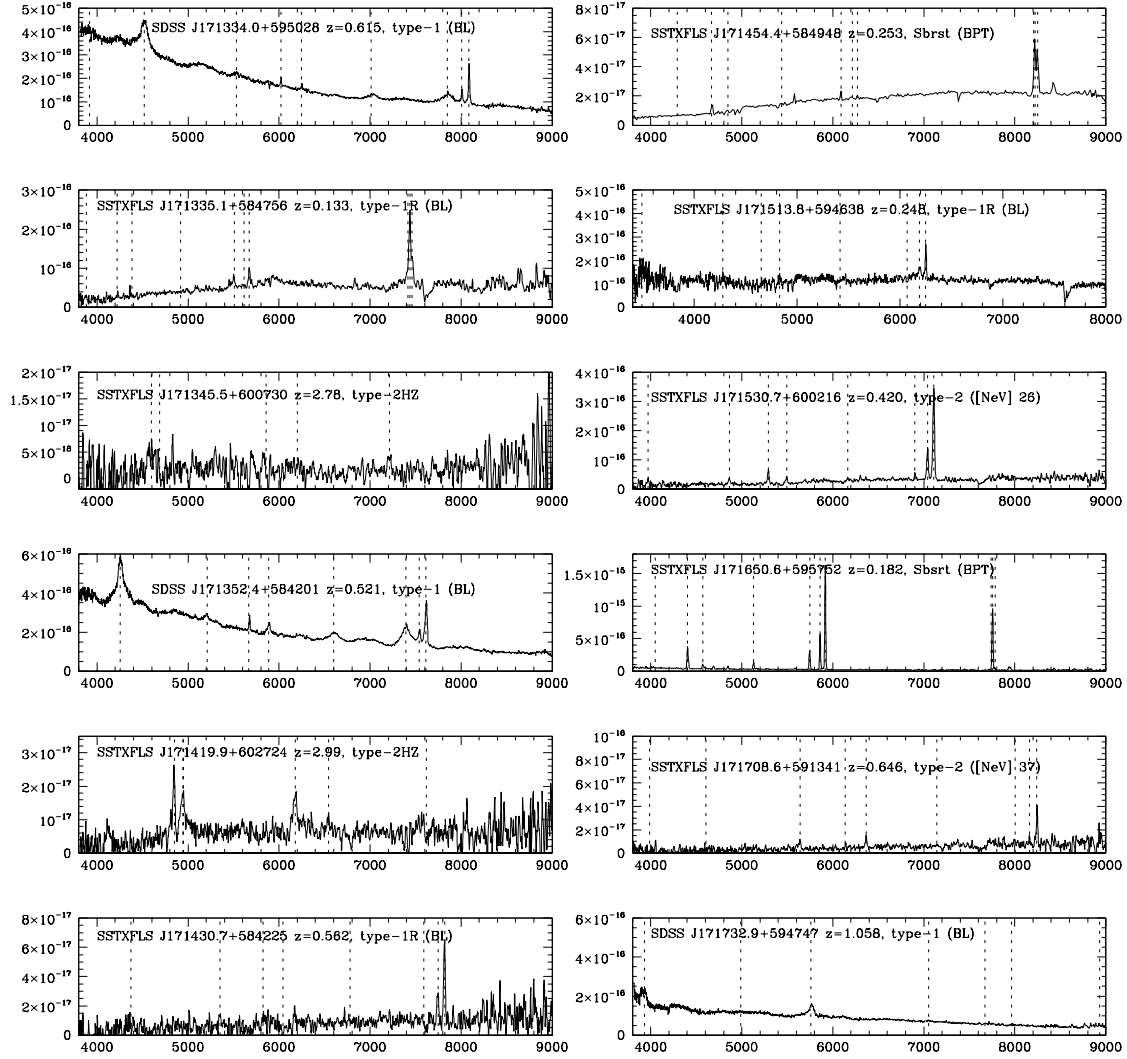


Fig. 2.— Optical spectra of the XFLS AGN candidates, continued

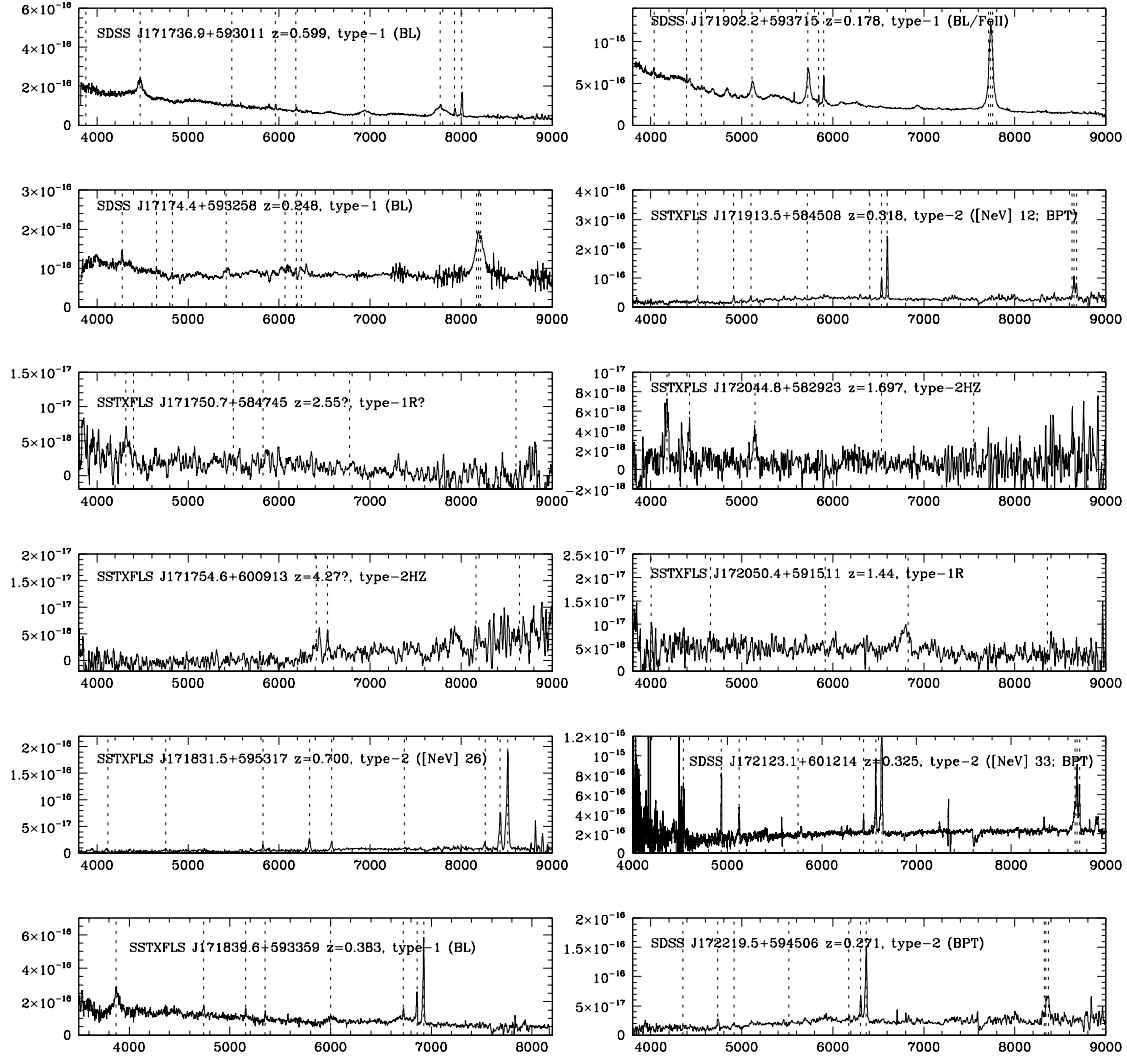


Fig. 2.— Optical spectra of the XFLS AGN candidates, continued

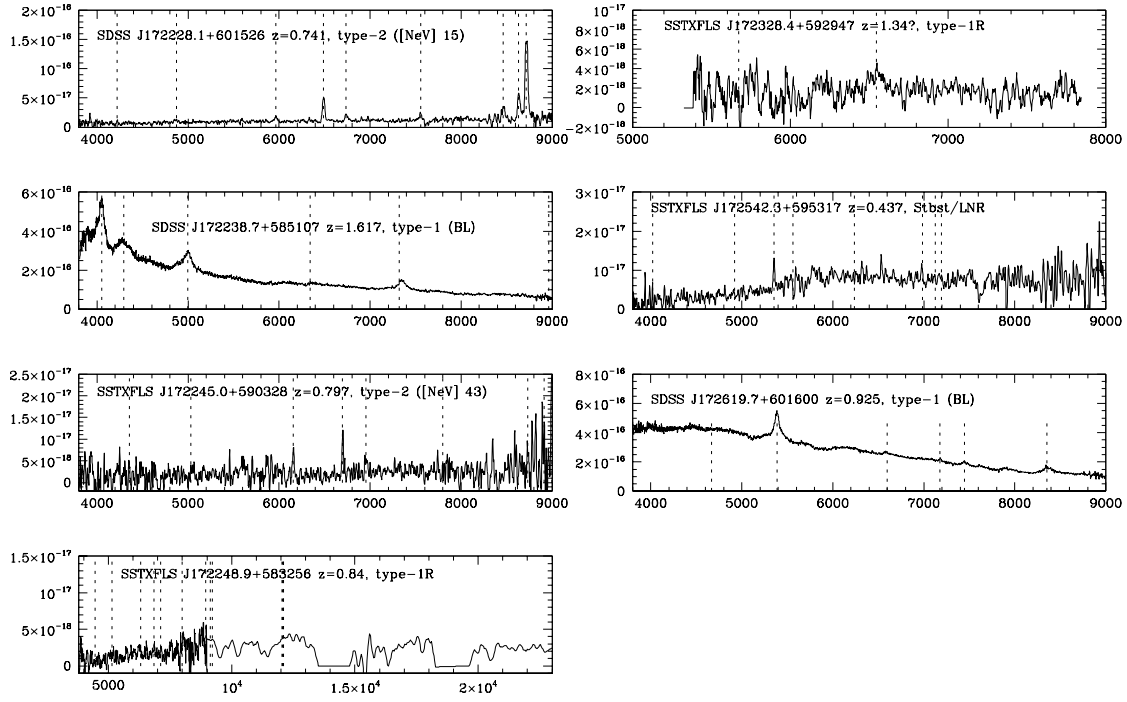


Fig. 2.— Optical spectra of the XFLS AGN candidates, continued

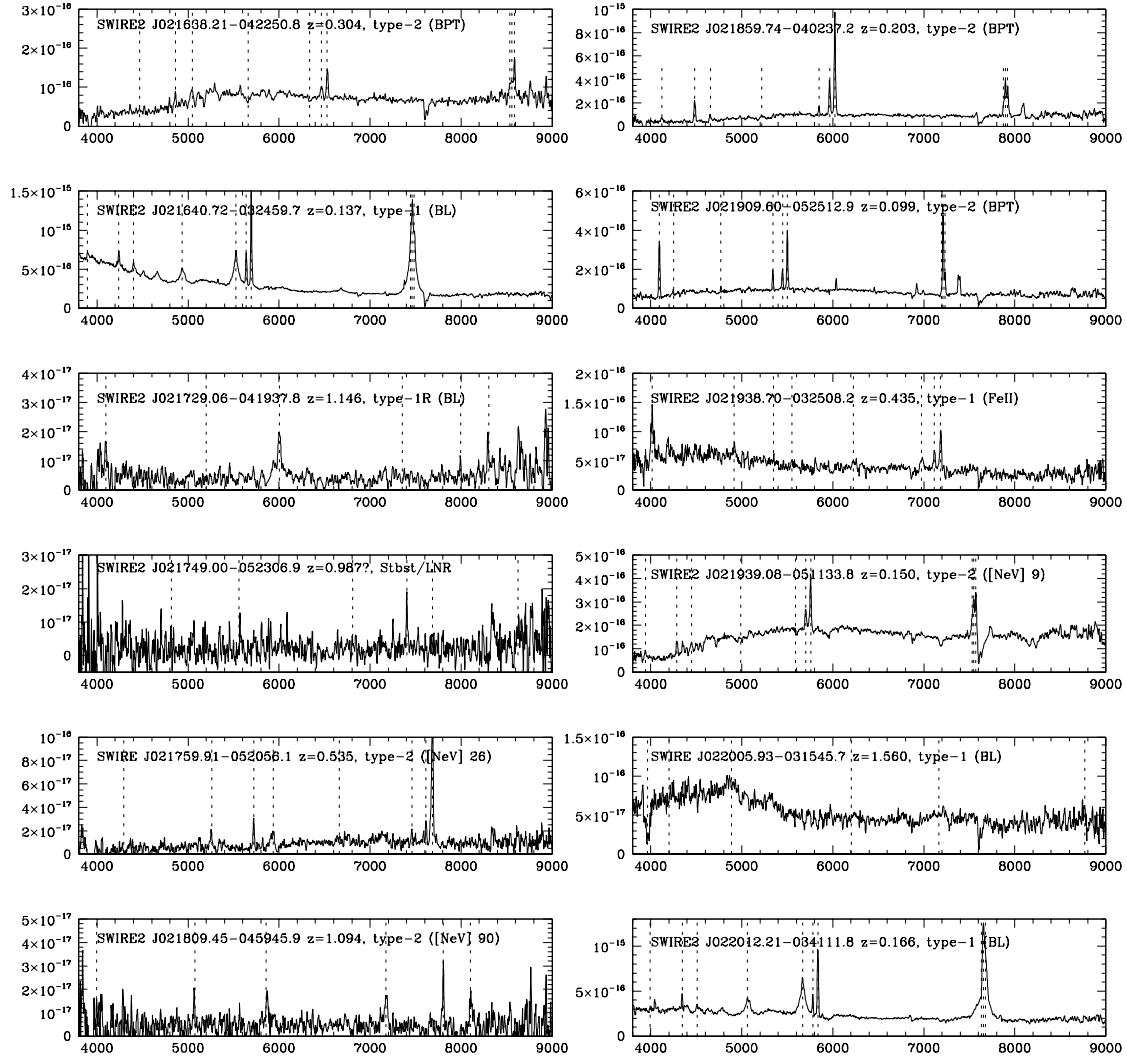


Fig. 3.— Optical spectra of the SWIRE AGN candidates. The position of emission lines are indicated as described in the caption to Figure 2. The spectra are presented in order of Right Ascension.

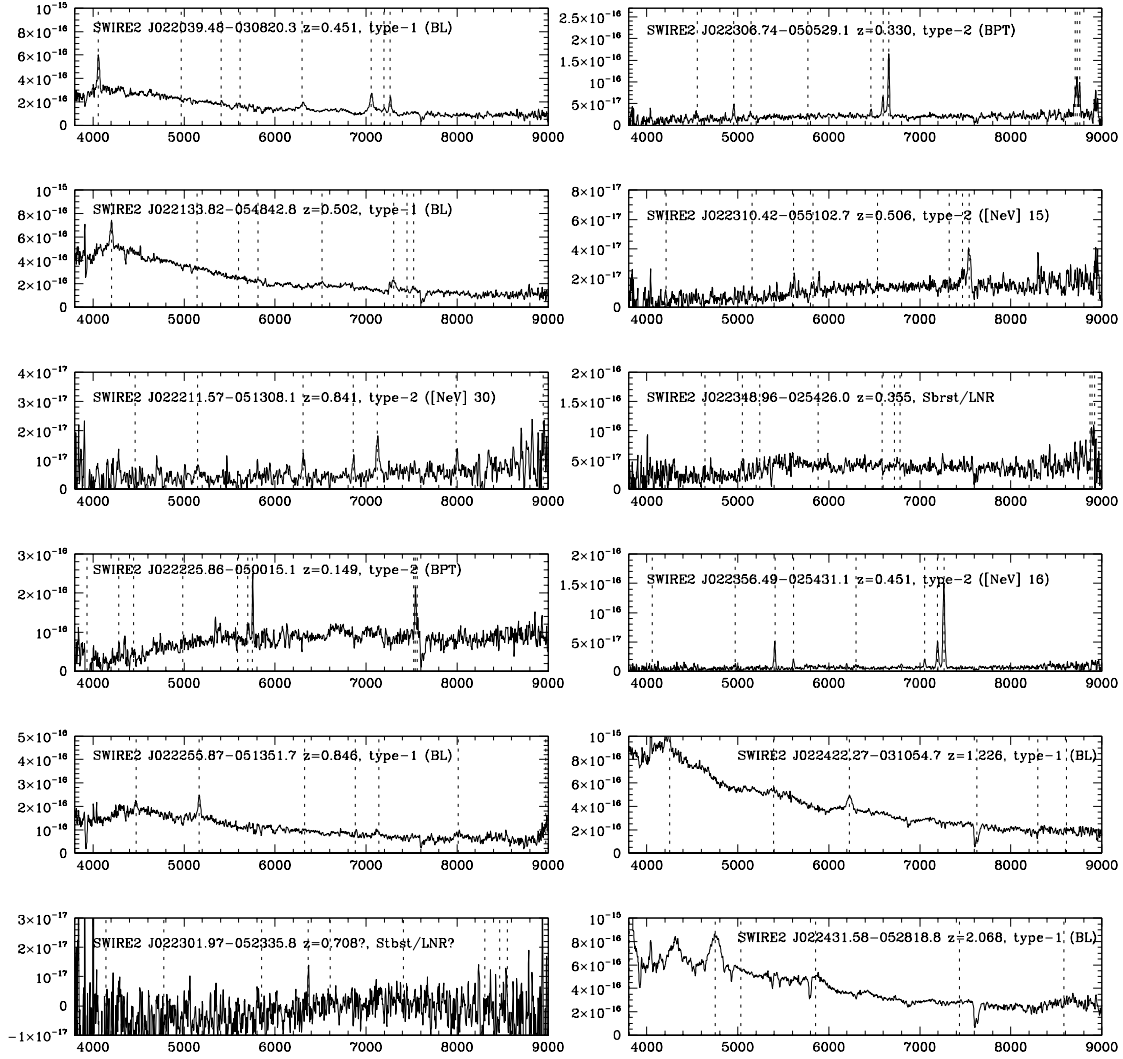


Fig. 3.— Optical spectra of the SWIRE AGN candidates, continued

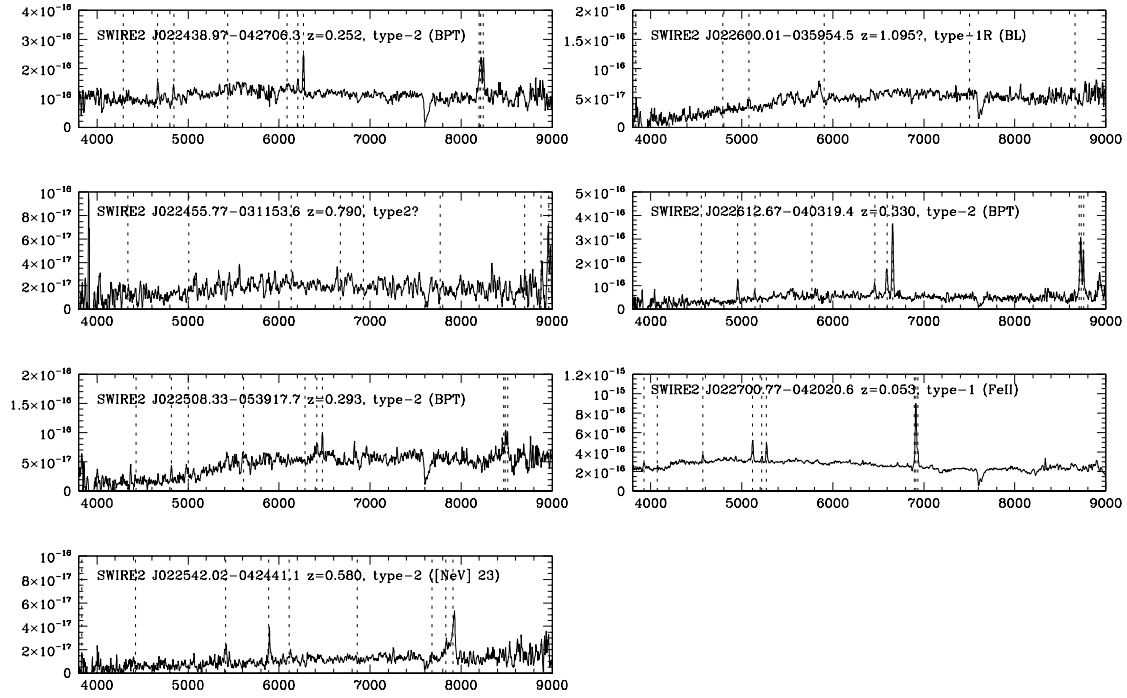


Fig. 3.— Optical spectra of the SWIRE AGN candidates, continued

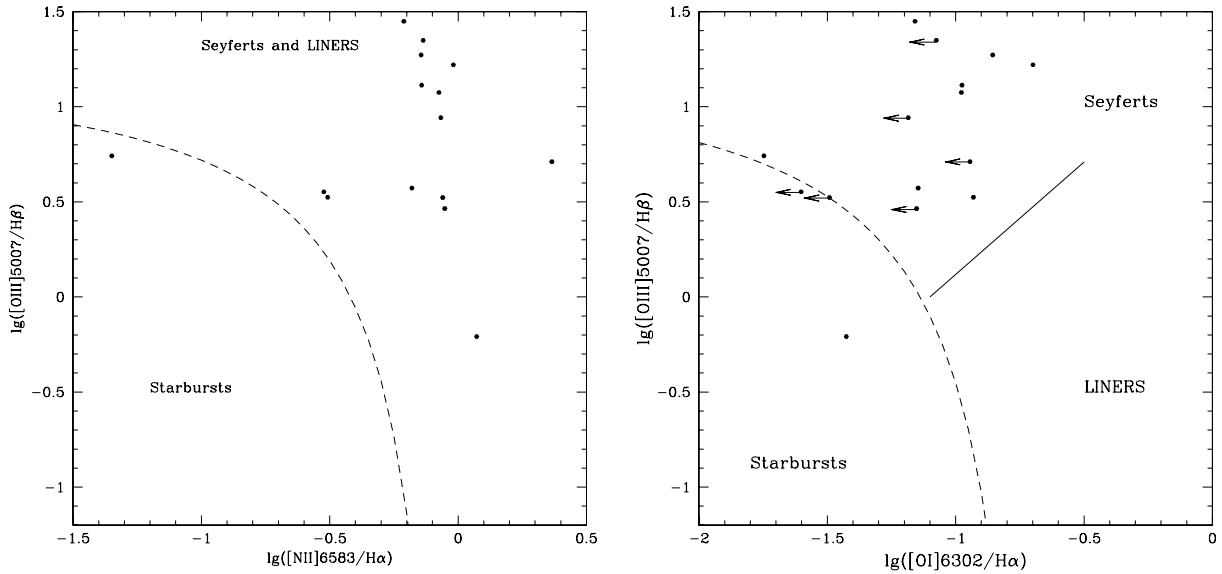


Fig. 4.— Two diagnostic (BPT) diagrams for our lower redshift emission line galaxies that have  $H\alpha$  in the optical window. The dividing lines are from Kewley et al. (2006). Most of our objects plot amongst the AGN, there are no LINERS in the sample.

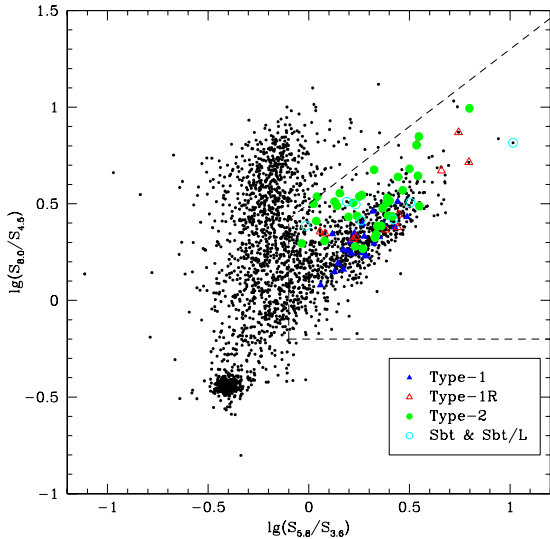


Fig. 1.— IRAC color-color plot for the XFLS field for objects detected in MIPS  $24\mu\text{m}$  and all four IRAC bands. The region within the dashed line is that used to select AGN. Objects in the AGN samples (both XFLS and SWIRE) are plotted as colored symbols. Object classifications are discussed in Section 3.

ing broad lines in their optical spectra, but with a faint, presumably dust-reddened quasar continuum and/or clear host galaxy emission with no sign of a blue quasar continuum above the host galaxy light are classed type-1R. Objects with high-ionization narrow emission lines which cannot be produced in a pure starburst scenario are classed as type-2. Objects with starburst emission line ratios in emission line diagnostic diagrams (Baldwin, Phillips & Terlevich 1983; hereafter BPT), and/or low ionization spectra with strong Balmer lines are classed as starbursts (Sbt). Where we have a low-ionization spectrum with too few lines to plot on a diagnostic diagram, or are low ionization and have  $H\alpha$  beyond the range of the optical spectrum they are classed as starburst/LINER (Sbt/L). Details of the bases of our optical classifications are described below. It should be emphasized that these classes are based on the *observed*-frame optical spectra, the rest-frame optical spectra may give different classifications. The classifications are given in the final columns of Tables 3 and 4, together with their basis. Of our sample of 77 objects, we find 25 objects with type-1 optical spectra, 11 with type-1R, 34 with type-2, two with unambiguous starburst

spectra and five with spectra which could be from either starbursts or LINERs.

### 3.2. Type-1 objects

Objects with linewidths of at least one permitted emission line  $> 3000\text{km}^{-1}$  are classified as type-1s. These objects have “BL” in the classification basis columns in Tables 3 and 4. This is sufficient to distinguish most of the luminous quasars. However, as our sample spans a wide luminosity range, several of the lower luminosity, lower redshift type-1 objects have narrower permitted lines (including a couple of candidate narrow-line Seyfert-1 galaxies). We therefore use the presence of strong permitted lines ( $H\beta/[OIII]5007 > 0.5$ ) and FeII emission in the 4000-5500Å range to classify them as type-1. These objects have “FeII” in the basis columns. The division into normal type-1 or reddened, type-1R, quasars is also made. This is decided on one of two criteria. If the optical spectrum is quasar-like, with featureless continuum and broad emission lines, but the continuum appears significantly reddened ( $E(B - V) \gtrsim 0.3$ ) compared to that of a normal quasar (see section 3.5), then the object is classified as type-1R. Also, some low- $z$  objects were classed as type-1R if the optical spectrum contains broad lines, but host galaxy features are visible and the object is dominated by host galaxy light in the blue.

### 3.3. Type-2 objects

Objects without broad lines or FeII emission, but with high-ionization narrow lines are classified as follows. Objects with [Nev] detections with rest-frame equivalent width  $> 5\text{Å}$  are classed as type-2 with the basis column containing “[Nev]” and the measured rest-frame equivalent width in Angstroms (for comparison the [Nev] 3426 emission line in the SDSS composite quasar spectrum of Vanden Berk et al. (2001) has an EW of  $\approx 0.6\text{Å}$ ). For low redshift objects where  $H\alpha$  was included in the spectra, we have used BPT diagrams to classify the AGN. Figure 4 shows the emission line ratios of our objects plotted on two diagnostic diagrams using the divisions between star-forming, Seyfert and LINER galaxies proposed by Kewley et al. (2006). Most objects plot with the Seyferts, though two objects plot close to the AGN/starburst division line in

both plots, and are presumably composite starburst/AGN objects (SSTXFLS 171650.6+595752; SWIRE2 J022225.86-050015.1). We class these as type-2 as they do have evidence of AGN activity, even if this is not dominating their optical emission line ratios. For some objects with neither [Nev] nor  $H\alpha/[NII]$  detected in their spectra we have relied on the ionization parameter as an approximate AGN indicator and used the  $[OIII]5007/[OII]3727$  ratio, classing objects with  $[OIII]5007/[OII]3727 > 1$  as questionable type-2s.

There are also a few high redshift objects having high-ionization UV permitted lines with widths  $\sim 2000\text{kms}^{-1}$ . Linewidths of this order are seen in the UV spectrum of NGC1068 (Grimes et al. 1999). Given this, and their high luminosities, we therefore anticipate that the true broad line widths will be much higher, so we are probably seeing only the narrow-line region in our spectra. However, given their high redshifts ( $z > 1.5$ ), only a very small amount of extinction is required to hide the broad-line region in the rest-frame UV. For the three highest redshift objects, at 2.78, 2.99 and 4.27, the rest-frame optical to near-infrared light is sampled in the IRAC bands, and this must almost certainly be dominated by reddened quasar light for these objects to exceed our IRAC flux limits. It is therefore unclear whether these objects should be classed as type-2s (showing no strong broad emission lines or quasar continuum in the rest-frame optical), or as class 1Rs. We thus assign  $z > 1.5$  objects with narrow UV lines class 2HZ (and group them with the type-2 objects for plotting and statistical purposes), pending better information on their rest-frame optical emission line properties and SEDs from near infrared imaging and spectroscopy. In all of these objects,  $Ly\alpha$  is typically faint compared to the high ionization UV lines, probably due to absorption by neutral hydrogen (e.g. van Ojik et al. 1994).

### 3.4. Starbursts and LINERs

We are left with seven objects with low-ionization lines, showing no signs of obvious AGN activity. Such objects have been classified as “type-3” AGN by Leipski et al. (2005). They are all relatively low redshift ( $z < 0.6$ ). All show [OII]3727 in emission, and Balmer absorption features. One also shows strong narrow  $H\beta$  and  $H\gamma$  emission. The two objects we have been able to

positively identify as starburst in the optical have been classified as such. The remainder are classified as starbursts/LINERs. Note that we fail to find any unambiguous LINERs in our sample. (SSTXFLS 171454.4+584948 plots below the Seyferts in the  $N[\text{II}]/\text{H}\alpha$  vs  $[\text{OIII}]/\text{H}\beta$  diagram, in the traditional LINER region [e.g. Kauffmann et al. 2003] but well within the starbursts in the  $[\text{OI}]/\text{H}\alpha$  vs  $[\text{OIII}]/\text{H}\beta$  diagram which gives a better discrimination of LINERs according to Kewley et al. [2006], so we have classified it as a starburst.) This may be due to LINERs lacking a substantial hot torus bright enough to dominate the mid-infrared over stellar emission (e.g. Ogle et al. 2006), but better spectra of our starburst/LINER objects are needed to confirm this.

For the most part our classifications are consistent with those of Papovich et al. (2006), though there are some objects which are differently classified. These are discussed in Appendix A.

### 3.5. Optical to mid-infrared color

In Figure 5 we show the observed  $R - [8.0]$  color plotted against redshift for the different spectral classifications. For the XFLS sample, the  $R$  magnitudes are from the survey of Fadda et al. (2004), those for the SWIRE sample are from the Cambridge Automatic Plate Measuring (APM) scans of the UK Schmidt Telescope plates (though in a few cases of faint or blended sources the magnitudes have been estimated by eye from digitized sky survey plates). Apart from a couple of low redshift AGN, which probably have their optical emission dominated by their host galaxies, all the normal type-1 objects trace the expected color locus for type-1 quasars very well, particularly the “IR luminous” SED of Richards et al. (2006), suggesting that the mid-infrared selection is not picking a very unusual population of type-1 quasars, but rather is finding quasars with the properties that we would expect from a sample selected in the mid-infrared. After the host galaxy contribution to the  $R$ -band becomes negligible at  $z \gtrsim 0.4$ , the normal and obscured (type 1R, 2 and 3) quasars separate, with very few objects having moderately-red colors. This relatively clean separation shows that our optical spectral classifications are indeed likely to be correct.

The  $z > 1.5$  type-2 objects (type 2HZ in Table 3), which have intermediate UV linewidths

and whose precise optical classification is therefore unclear, are obviously redder than the expected mid-infrared to optical color of normal quasars at these redshifts, suggesting that they are not simply quasars with unusually narrow lines, but do indeed have most of their nuclear emission extinguished by dust.

Our division between type-1 and type-1R quasars also appears to be justified on the basis of this color (at least for objects at  $z \gtrsim 0.4$  where the host galaxy does not affect the  $R$ -magnitude), with the type-1R quasars having rest-frame reddenings  $E(B - V) \sim 0.3 - 0.7$ .

## 4. X-ray detections

There is some overlap between objects in the SWIRE-XMM fields and archival *XMM-Newton* data. 21 of 34 sources in the SWIRE-XMM sample fall on moderately deep (5-50ks) XMM exposures. These are sufficiently deep to detect, or to set useful limits on, the X-ray flux from our sources. These data appear to have been taken for several different surveys, including the *XMM* large-scale structure survey (e.g. Chiapetti et al. 2005) and the the Subaru *XMM-Newton* Deep Survey (SXDS; Watson et al. 2004). We have obtained approximate fluxes for these objects in order to investigate the optical-to-X-ray luminosity ratios of our sources (Table 5). This allows us to place our mid-infrared selected obscured AGN into the context of X-ray samples of similar objects. Counts in the 0.2-12keV range from the PN detector of the European Photon Imaging Camera (EPIC), as listed in the 1XMM serendipitous catalog (e.g. Michel et al. 2004), or the pre-release of the 2XMM catalogue (The Second XMM-Newton Serendipitous Source Pre-release Catalogue, XMM-Newton Survey Science Centre) have been used where available, otherwise counts have been taken from the source lists available from the XMM archive (the pipeline products [PPS] lists). Limits are estimated from the fluxes of the faintest believable detections on each image, and correspond to  $\approx 3\sigma$ . Fluxes from the 1XMM or 2XMM catalogs are from the PN countrate in 1XMM, and from the average over all detectors in 2XMM. Where only counts or a limit are available fluxes are derived from the count rate using the PIMMS website (<http://heasarc.gsfc.nasa.gov/Tools/w3pimms.html>),

Table 3: Bright AGN in the XFLS region

Name	$S_{24.0}/\text{mJy}^1$	Redshift	Class	Basis
SDSS J171033.1+584456	6.1	0.281	1R	FeII/BL
SSTXFSL J171115.2+594906	9.4	0.587	Sbt	strong Balmer lines
SDSS J171117.6+584123	5.8	0.617	1	BL
SDSS J171124.2+593121	5.5	1.491	1	BL (LoBAL?)
SSTXFSL J171147.4+585839	4.8	0.800	2	[Nev]13
SDSS J171207.4+584754	13.4	0.269	1	FeII
SSTXFSL J171233.4+583610	5.1	1.663	1R	BL
SSTXFSL J171302.3+593610	11.8	0.668	2	[Nev]33
SSTXFSL J171313.9+603146	10.5	0.124	2	BPT
SSTXFLS J171324.2+585549	4.9	0.609	2	[Nev]12
SSTXFSL J171325.1+590531	9.5	0.126	2	BPT
SSTXFSL J171331.5+585804	5.9	0.435	Sbt/L	[OIII]/[OII]<1
SDSS J171334.0+595028	5.4	0.615	1	BL
SSTXFSL J171335.1+584756	23.7	0.133	1R	FeII
SSTXFSL J171345.5+600730	4.9	2.78	2HZ	narrow UV lines
SDSS J171352.4+584201	23.9	0.521	1	BL/FeII
SSTXFSL J171419.9+602724	5.6	2.99	2HZ	narrow UV lines
SSTXFSL J171430.7+584225	8.2	0.561	1R	BL <sup>†</sup>
SSTXFLS J171454.4+584948*	4.9	0.253	Sbt	BPT
SSTXFLS J171513.8+594638	5.0	0.248	1R	BL (radio-loud)
SSTXFSL J171530.7+600216	11.6	0.420	2	[Nev]26
SSTXFSL J171650.6+595752	6.7	0.182	2	BPT (composite)
SSTXFSL J171708.6+591341	5.4	0.646	2	[Nev]37
SDSS J171732.9+594747	4.6	1.058	1	BL
SDSS J171736.9+593011	6.4	0.599	1	BL
SDSS J171747.4+593258	5.4	0.248	1	BL
SSTXFSL J171750.7+584745	5.1	2.55?	1R?	BL?
SSTXFSL J171754.6+600913	8.9	4.27	2HZ	narrow UV lines
SSTXFSL J171831.5+595317	8.3	0.700	2	[Nev]26
SSTXFSL J171839.6+593359	10.9	0.383	1	BL (radio loud)
SDSS J171902.2+593715	26.9	0.178	1	BL/FeII
SSTXFSL J171913.5+584508	8.9	0.318	2	[Nev]12, BPT
SSTXFSL J172044.8+582923	5.1	1.697	2HZ	narrow UV lines
SSTXFSL J172050.4+591511	9.4	1.44	1R	BL
SSTXFSL J172123.1+601214	13.3	0.325	2	[Nev]33/BPT
SSTXFSL J172219.5+594506	7.8	0.271	2	BPT
SSTXFSL J172228.1+601526	7.1	0.741	2	[Nev]15
SDSS J172238.7+585107	6.7	1.617	1	BL
SSTXFSL J172245.0+590328	4.7	0.797	2	[Nev]43
SSTXFSL J172248.9+583256	5.6	0.84	1R	BL
SSTXFSL J172328.4+592947	8.1	1.34?	1R	BL
SSTXFSL J172542.3+595317	9.5	0.437	Sbt/L	low ionization
SDSS J172619.7+601600	6.6	0.925	1	BL

\* Spectrum from Papovich et al. (2006).

<sup>†</sup> classification based on Papovich et al. spectrum, see Appendix A. <sup>‡</sup> Optical/near-IR redshift is uncertain, but a *Spitzer* mid-IR spectrum shows silicate absorption at  $z = 0.84$  (Lacy et al. 2006, in preparation).

Table 4: Bright AGN in the SWIRE-XMM region

Name	$S_{24.0}/\text{mJy}^1$	Redshift	Class	Basis
SWIRE2 J021638.21-042250.8	14.6	0.304	2	BPT
SWIRE2 J021640.72-044405.1	14.8	0.870	1	Becker et al. (2001)
SWIRE2 J021657.77-032459.7	24.2	0.137	1	BL
SWIRE2 J021729.06-041937.8	8.9	1.146	1R	BL
SWIRE2 J021749.00-052306.9	8.1	0.987?	Sbt/L?	low ionization?
SWIRE2 J021759.91-052056.1	8.8	0.535	2	[Nev]26
SWIRE2 J021808.22-045845.3	9.2	0.712	1	Caccianiga et al. (2004)
SWIRE2 J021809.45-045945.9	7.8	1.094	2	[Nev]90
SWIRE2 J021830.57-045622.9	8.5	1.401	1	Sharp et al. (2002)
SWIRE2 J021859.74-040237.2	16.0	0.203	2	BPT
SWIRE2 J021909.60-052512.9	25.6	0.099	2	BPT
SWIRE2 J021938.70-032508.2	6.6	0.435	1	FeII
SWIRE2 J021939.08-051133.8	32.9	0.150	2	[Nev]9
SWIRE2 J022005.93-031545.7	6.6	1.560	1	BL
SWIRE2 J022012.21-034111.8	6.8	0.166	1	BL
SWIRE2 J022039.48-030820.3	10.6	0.451	1	BL
SWIRE2 J022133.82-054842.8	6.9	0.502	1	BL
SWIRE2 J022211.57-051308.1	6.7	0.841	2	[Nev]30
SWIRE2 J022225.86-050015.1	8.3	0.149	2	BPT (composite)
SWIRE2 J022255.87-051351.7	8.3	0.846	1	BL
SWIRE2 J022301.97-052335.8	6.8	0.708?	Sbt/L?	low ionization?
SWIRE2 J022306.74-050529.1	16.0	0.330	2	BPT
SWIRE2 J022310.42-055102.7	13.3	0.506	2	[Nev]15
SWIRE2 J022348.96-025426.0	7.6	0.355	3	low ionization
SWIRE2 J022356.49-025431.1	10.6	0.451	2	[Nev]16
SWIRE2 J022422.27-031054.7	7.8	1.226	1	BL
SWIRE2 J022431.58-052818.8	9.4	2.068	1	BL
SWIRE2 J022438.97-042706.3	6.6	0.252	2	BPT
SWIRE2 J022455.77-031153.6	7.6	0.790	2?	[OIII]/[OII]>1
SWIRE2 J022508.33-053917.7	9.6	0.293	2	BPT
SWIRE2 J022542.02-042441.1	10.9	0.580	2	[Nev]23
SWIRE2 J022600.01-035954.5	9.0	1.095?	1R	BL
SWIRE2 J022612.67-040319.4	7.7	0.330	2	BPT
SWIRE2 J022700.77-042020.6	27.1	0.053	1	FeII

assuming an input spectrum with photon index of two and a column of  $10^{21}\text{cm}^{-2}$ .

A few points are clear from even this preliminary study. All the type-1 quasars are detected in the X-ray (albeit with about an order of magnitude of scatter in their X-ray to infrared ratios), but only about half of the optically-obscured quasars (Figure 6). The obscured quasars do, however, show a wide range in X-ray to infrared flux ratios, ranging from little or no absorption to X-ray fluxes absorbed by a factor of ten or more (averaged over the 0.2-12keV band) relative to the type-1s. Interestingly, one of the two starburst/LINER objects in these X-ray fields is detected, though the other is not.

## 5. Discussion

### 5.1. Selection effects and redshift biases

Every technique for selecting AGN is affected by selection biases, and this one is no exception. The color selection means that objects whose observed mid-infrared colors are not dominated by thermal emission from the AGN will be missing from the sample. This can happen in a variety of ways. First, the AGN may simply be of such low luminosity in the infrared that the starlight from the host galaxy dominates the mid-infrared emission, either because the AGN is intrinsically weak, or because the covering factor of the hot dust is low, perhaps because of an unusual torus geometry. This bias gets worse with increasing redshift as the stellar bump in the rest-frame near-infrared is redshifted into the mid-infrared bands, and the  $k$ -correction on the thermal emission of the dust becomes large. Second, some AGN will simply be so highly-obscured that the AGN emission is not seen at observed wavelengths  $< 8\mu\text{m}$ . Third, some AGN may also be so highly obscured that they drop out of the IRAC catalogs at short wavelengths.

The positions of the different classes of objects within the “AGN wedge” on the IRAC color-color plot of Figure 1, shown in detail in Figure 7, can give us some idea of the particular selection effects for each class of object. The type-1 quasars all lie in a fairly tight group in the center of the wedge, so few are likely to be missing (see also Paper 1). Reddened type-1s show more dispersion, including two with very red IRAC colors. The type-

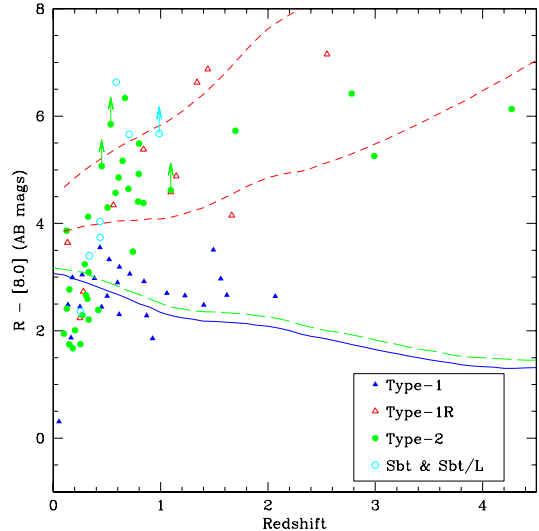


Fig. 5.— Optical to infrared color for our quasar samples. Type-3 objects which lack redshifts have been assigned a redshift of 1.50. The color loci of two of the quasar SEDs of Richards et al. (2006) are plotted as lines. The blue solid line is the mean quasar SED and the green long-dashed line the “IR luminous” SED. The red dashed lines indicate the colors of the mean quasar SED reddened by the Small Magellanic Cloud extinction law of Pei (1992). The lower line corresponds to a rest-frame reddening of  $E(B - V) = 0.32$  and the upper to 0.65. The dispersion in optical to mid-IR color of the quasars of Richards et al. (2006) is  $\approx \pm 0.3$  mag.

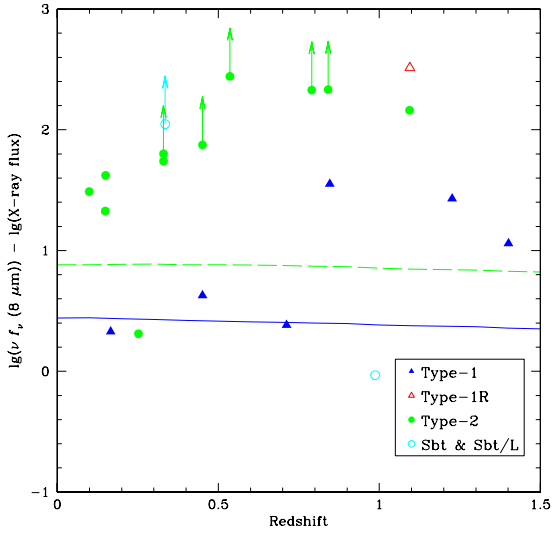


Fig. 6.— Observed X-ray (0.2-12 keV) flux versus observed  $8.0\mu\text{m}$  infrared flux ratios for objects in archival XMM fields. The blue solid line is the mean quasar SED of Richards et al. extrapolated from the soft X-ray assuming a photon index of 1.8, the green dashed line the same for the “IR luminous” SED.

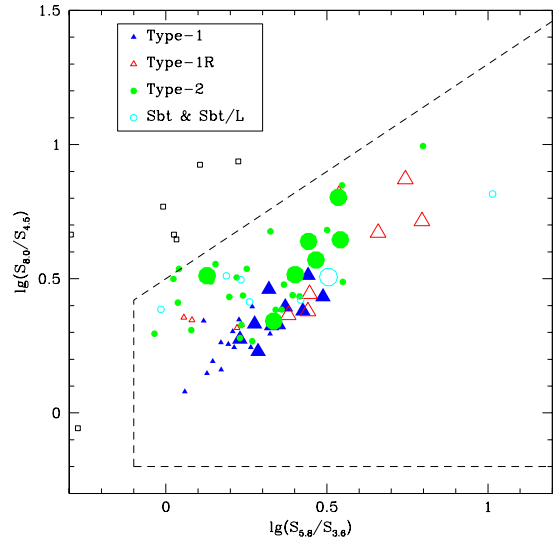


Fig. 7.— Enlarged view of the “AGN wedge” of Figure 1. Large symbols represent  $z \geq 0.8$  objects, small symbols those at  $z < 0.8$ . Open squares represent the objects from the sample of Table 6 which have AGN-like optical emission line ratios but non-AGN IRAC colors.

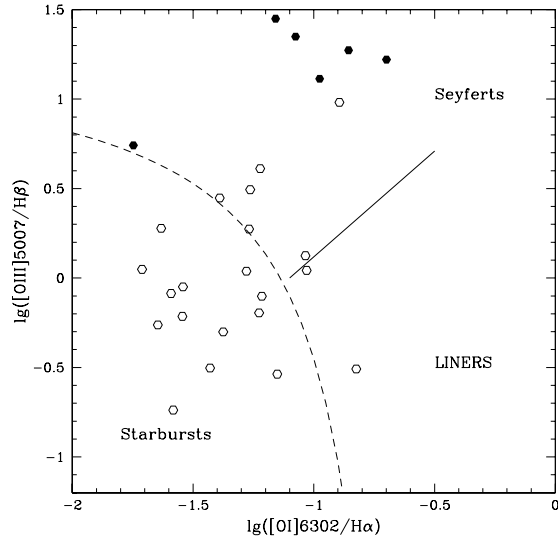


Fig. 8.—  $[\text{OI}]/\text{H}\alpha$  vs  $[\text{OIII}]/\text{H}\beta$  BPT diagram for the objects of Table 6 (the 50 brightest  $24\mu\text{m}$  sources, regardless of IRAC colors) with  $[\text{OIII}]$  detections. Objects falling outside of the IRAC AGN color selection are shown as open symbols, those within it as closed.

2s are also more dispersed, with several (mostly low redshift objects) trending towards the diagonal divide in the color-color plot, presumably due to PAH emission, and several with very red colors. The starbursts and starburst/LINERs are surprisingly close to the center of the wedge, though one does have extremely red IRAC colors. From Figure 7 we can deduce that some (probably mostly lower- $z$ ) type-2 objects are probably missing due to plotting with the PAH-dominated galaxies, and that all classes of obscured quasars are probably missing their reddest representatives. There is a weak trend whereby the higher redshift objects tend to be located towards redder colors in the wedge, though at the highest redshifts, where the IRAC colors are sampling the rest-frame optical and near-infrared, the colors become bluer again.

As these selection effects have yet to be modeled in depth, we will defer further discussion to a later paper, where we will attempt to model the emission from our objects in detail and apportion luminosity between AGN and starburst components (Petric et al. 2006). However, we point out here that our fraction of obscured quasars is necessarily a lower limit, and this limit becomes increasingly poor with increasing redshift.

## 5.2. Objects with low ionization optical spectra

Are there any high luminosity AGN in which both the broad and narrow-line regions are obscured, or otherwise missing? This study has found several objects which qualify as “type-3” quasars (following Leipski et al. [2005]), namely galaxies with emission line properties more typical of LINER or starburst galaxies than narrow-line AGN. Leipski et al. find 57% of their ISO/2MASS selected AGN have these optical spectra. Martínez-Sansigre et al. (2005, 2006) also deduce the presence of a significant population of obscured narrow-line AGN from their mid-infrared/radio selected objects which show no emission lines in the rest-frame UV.

Our study has a lower fraction. Including both objects with starburst or ambiguous starburst/LINER spectra we find a “type-3” fraction of  $\approx 9\%$ , which is of course an upper limit as, apart from one case which is detected in the X-ray at the level expected for an AGN (SWIRE2 J021749.00-052306.9), we cannot prove the presence of AGN

in these objects. Thus, despite the inferred presence of hot dust, infrared spectroscopy or X-ray detection (at a level greater than expected for a starburst) is required to prove the AGN nature of these candidate type-3 objects. If they are reddened AGN, the reddening may be in the host (e.g. Martínez-Sansigre et al. 2005; Rigby et al. 2006), though we cannot eliminate the possibility that nuclear dust is obscuring the narrow-line region, or is blocking the line of sight to the narrow line region from the nucleus.

X-ray surveys too find a population of AGN which lack optical evidence for AGN activity, the X-ray bright, optically-normal galaxies (XBONGs) (e.g. Comastri et al. 2002). A number of processes have been suggested for the lack of optical AGN activity in these objects, including host galaxy obscuration (Rigby et al. 2006), radiatively inefficient accretion (Yuan & Narayan 2004) or dilution of weak emission lines by host galaxy light (Moran, Filippenko & Chornock 2002; Eckhart et al. 2006). The discovery of [Nv]3426 emission in a stacked spectrum of XBONGs made by Eckart et al. (2006) favors dilution and/or extinction over a fundamental difference in accretion mode. The same may well be true if our type-3 quasars really are AGN, particularly any that are composite starburst/AGN systems with strong star formation activity in the host galaxies. In particular, objects which are classified on the basis of line ratios in the BPT diagram may have their AGN line emission overwhelmed by the starburst component, which is likely to dominate the overall energetics of the galaxy.

Dilution of AGN signatures by host galaxy emission may help to explain why our type-3 fraction is lower than those of Leipski et al., whose objects are mostly of lower redshift and luminosity, where host galaxy contamination is more of an issue. Our type-3 fraction may be smaller than that of Martínez-Sansigre et al. (2005, 2006) due to our order of magnitude brighter flux limit at  $24\mu\text{m}$  allowing us to find more objects with intrinsically faint or lightly-reddened ( $E(B-V) \sim 0.1-1$ ) narrow lines. Certainly it is apparent from our spectroscopic campaign that even objects with  $24\mu\text{m}$  fluxes of several mJy can require 1.5hrs of integration on a 5m telescope to see emission lines.

Table 5: XMM-Newton detections of AGN in the SWIRE field

Object name	$z$	Opt class	Obs ID name	Exposure time	Camera	counts	source	$S_{0.2-12\text{keV}}$ ( $10^{-14}$ $\text{ergs}^{-1}\text{cm}^{-2}$ )
SWIRE2 J021749.00-052306.9	0.987?	Sbt/L??	0112370701	47648	PN	20050	2XMM	178
SWIRE2 J021759.91-052056.1	0.535	2	0112370801	47330	PN	$\lesssim 50$	PPS	$\lesssim 0.4$
SWIRE2 J021808.22-045845.3	0.712	1	0112370101	57631	PN	14500	1XMM	104
SWIRE2 J021809.45-045945.9	1.094	2	0112370101	57631	PN	100	PPS	0.75
SWIRE2 J021830.57-045622.9	1.401	1	0112370101	57631	PN	3100	1XMM	22
SWIRE2 J021909.60-052512.9	0.099	2	0112370801	47330	PN	300	2XMM	2.6
SWIRE2 J021939.08-051133.8	0.150	2	0112370801	47330	PN	601	1XMM	5.3
SWIRE2 J022012.21-034111.8	0.166	1	0037982601	11592	PN	1740	2XMM	63
SWIRE2 J022039.48-030820.3	0.451	1	0037982701	14892	PN	1100	2XMM	31
SWIRE2 J022211.57-051308.1	0.841	2	0111110501	20056	PN	$\lesssim 20$	PPS	$\lesssim 0.4$
SWIRE2 J022225.86-050015.1	0.149	2	0111110501	20056	MOS2	30	PPS	2.0
SWIRE2 J022255.87-051351.7	0.846	1	0111110501	20056	PN	20	1XMM	22
SWIRE2 J022306.74-050529.1	0.330	2	0111110501	20056	PN	46	1XMM	0.95
SWIRE2 J022348.96-025426.0	0.355	Sbt/L	0037981601	13319	PN	$\lesssim 26$	PPS	$\lesssim 0.8$
SWIRE2 J022356.49-025431.1	0.451	2	0037981601	13319	PN	$\lesssim 26$	PPS	$\lesssim 0.8$
SWIRE2 J022422.27-031054.7	1.226	1	0037981201	8420	PN	170	2XMM	8.4
SWIRE2 J022438.97-042706.3	0.252	2	0112680501	10040	PN	1600	2XMM	30
SWIRE2 J022455.77-031153.6	0.790	2?	0037981301	5702	PN	$\lesssim 10$	PPS	$\lesssim 0.8$
SWIRE2 J022542.02-042441.1	0.580	2	0112681001	41946	PN	$\lesssim 442$	PPS	$\lesssim 0.4$
SWIRE2 J022600.01-035954.5	1.095?	1R	0112680201	13675	PN	33	2XMM	1.0
SWIRE2 J022612.67-040319.4	0.330	2	0112680201	13675	PN	$\lesssim 27$	PPS	$\lesssim 0.8$

### 5.3. Reliability and effectiveness of mid-infrared selection of AGN

The IRAC color technique is clearly effective at selecting AGN, at least for objects with fluxes of a few mJy at  $24\mu\text{m}$ . We have been able to unambiguously classify most of our objects as AGN based on their optical spectra. Contaminants are certainly possible, however. At moderate redshift, starbursts will be able to move into the AGN “wedge” if they have large amounts of warm dust, and at high redshifts, the  $1.6\mu\text{m}$  bump of stellar SEDs can lead to IRAC colors which mimic those of AGN. We can state that for this sample of 77 bright  $24\mu\text{m}$  sources, only seven lack obvious optical signatures of AGN activity, and of these, one is detected in an XMM field, which implies a contamination rate of  $< 6/77$  (8%).

Of course, the selection of bright  $24\mu\text{m}$  sources itself produces a large fraction of AGN, as demonstrated by Brand et al. (2006). In particular, when combined with optical photometric criteria, a sample containing a large fraction of AGN can be made by simply rejecting the optically-bright objects. To investigate how effective such a cut is, and to take a first look at the completeness of our AGN sample, we have examined the brightest 50 sources in the XFLS  $24\mu\text{m}$  list (Table 6). This

sample contains 29 objects which are classed as AGN according to the criteria of Section 3. As the starbursts are also concentrated to lower redshifts, this qualitatively confirms the result of Brand et al. (2006), namely that the mid-infrared luminosity density is dominated by AGN at mJy flux levels. Objects with faint optical identifications are certainly more likely to be AGN - no object with  $R > 21$  is classified as a starburst or LINER, but apart from that division there is a wide range in magnitudes ( $R \approx 17 - 20$ ) over which AGN and starburst/LINERs overlap, particularly if no optical morphology criterion is used and thus quasars are included.

This sample of the 50 brightest  $24\mu\text{m}$  sources also allows us to take a first look at how complete the AGN selection using IRAC colors is. Interestingly, we find that seven objects outside the IRAC color-based AGN selection show AGN-like emission line ratios in a BPT diagram, though these are nearly all close to the AGN-starburst transition region (Figure 8). Their positions in the IRAC color-color plot are shown in Figure 7. In six of these cases IRAC  $8.0\mu\text{m}$  band flux is very high, pushing the objects into the starforming galaxy region of the color-color plot of Figure 1. The remaining object (SSTXFLS J171150.2+590041) shows pure Seyfert emission line ratios, but has only a weak

Table 6: The 50 brightest extragalactic  $24\mu\text{m}$  sources in the XFLS with 4-band IRAC coverage

Name	$S_{24}$ (mJy)	$R$	Spectrum <sup>‡</sup>	Redshift	Class	Basis	IRAC-selected AGN?
SSTXFLS J171115.2+594907	9.41	20.97	L06	0.587	Sbt	strong Balmer lines	yes
SSTXFLS J171150.2+590041	10.88	17.97	P06	0.060	2	BPT	no
SDSS J171207.4+584754	13.34	17.76	L06	0.269	1	FeII	yes
SSTXFLS J171232.3+592126	8.47	17.56	P06	0.21	Sbt/L	low ionization	no
SSTXFLS J171302.3+593611	11.83	21.50	L06	0.668	2	[Nev]33	yes
SSTXFLS J171313.9+603146	10.49	18.31	L06	0.105	2	BPT	yes
SSTXFLS J171325.1+590531	9.43	18.33	L06	0.126	2	BPT	yes
SSTXFLS J171335.1+584756	23.66	17.56	L06	0.133	1R	FeII	yes
SDSS J171352.4+584201	23.90	17.53	SDSS	0.521	1	BL/FeII	yes
SSTXFLS J171414.8+585221	8.97	18.70	P06	0.167	Sbt	BPT	no
SSTXFLS J171430.7+584225	8.24	19.72	L06	0.561	1R	BL	yes
SSTXFLS J171437.4+595647	11.60	18.75	P06	0.196	2	BPT (composite)	no
SSTXFLS J171446.4+593359	7.37	17.67	P06	0.129	Sbt/L	low ionization	no
SSTXFLS J171530.7+600216	11.55	18.82	L06	0.420	2	[Nev]26	yes
SDSS J171540.1+591647	6.88	17.43	SDSS	0.116	Sbt/L	low ionization	no
SSTXFLS J171542.0+591657	26.33	17.50	P06	0.116	Sbt	BPT	no
SSTXFLS J171544.0+600835	6.86	17.07	L06*	0.157	2	BPT	no
SDSS J171607.2+591456	34.57	16.27	SDSS	0.054	Sbt	BPT	no
SDSS J171614.4+595423	8.41	17.39	SDSS	0.153	Sbt	BPT	no
SDSS J171630.1+601423	8.35	17.82	SDSS	0.107	Sbt	BPT	no
SSTXFLS J171634.0+601443	10.76	17.04	P06	0.108	Sbt	BPT	no
SDSS J171635.9+601436	7.66	17.07	SDSS	0.106	Sbt	BPT	no
SDSS J171641.0+591857	20.88	16.41	SDSS	0.056	Sbt	BPT	no
SSTXFLS J171650.5+595751	6.69	18.81	L06	0.182	2	BPT (composite)	yes
SSTXFLS J171711.1+602710	9.43	17.88	L06*	0.110	Sbt/L	low ionization	no
SSTXFLS J171744.1+583848	13.92	17.73	P06	0.066	L	BPT	no
SSTXFLS J171754.6+600913	8.94	21.80	L06	4.27	2HZ	narrow UV lines	yes
SSTXFLS J171831.7+595317	8.27	20.56	L06	0.700	2	[Nev]26	yes
SSTXFLS J171839.7+593359	13.22	17.99	L06	0.383	1	BL	yes
SSTXFLS J171852.7+591432	13.92	19.23	P06	0.322	2/L	BPT	no
SSTXFLS J171902.2+593715	26.91	17.10	L06	0.178	1	BL/FeII	yes
SSTXFLS J171913.5+584509	8.90	19.00	L06	0.318	2	[Nev]12, BPT	yes
SSTXFLS J171916.6+593449	17.40	17.91	P06	0.166	2/L	BPT	no
SSTXFLS J171933.3+592742	7.53	17.71	P06	0.139	2	BPT (composite)	no
SDSS J171944.8+595705 <sup>†</sup>	6.73	16.66	SDSS	0.069	Sbt	BPT	no
SDSS J171944.9+595707 <sup>†</sup>	7.44	16.66	SDSS	0.069	Sbt	BPT	no
SSTXFLS J172028.9+584749	9.57	16.74	L06*	0.127	2	BPT	no
SDSS J172043.2+584026	9.48	17.08	SDSS	0.125	Sbt	BPT	no
SSTXFLS J172050.5+591512	9.41	21.62	L06	1.44	1R	BL	yes
SSTXFLS J172123.1+601214	13.34	18.78	L06	0.325	2	[Nev]33, BPT	yes
SSTXFLS J172219.5+594507	7.76	18.71	L06	0.272	2	BPT	yes
SSTXFLS J172220.2+590949	8.78	17.58	P06	0.179	Sbt	BPT	no
SSTXFLS J172228.0+601525	7.12	19.85	L06	0.741	2	[Nev]15	yes
SDSS J172238.7+585107	6.73	18.17	SDSS	1.617	1	BL	yes
SSTXFLS J172328.4+592947	8.10	22.15	L06	1.34?	1R	BL	yes
SSTXFLS J172400.6+590228	13.34	17.99	P06	0.178	Sbt	BPT	no
SDSS J172402.1+600601	7.76	17.12	SDSS	0.156	Sbt/L	low ionization	no
SSTXFLS J172508.8+591016	9.40	17.78	P06	0.164	Sbt	BPT	no
SSTXFLS J172542.3+595317	9.45	20.03	L06	0.437	Sbt/L	low ionization	yes
SSTXFLS J172619.7+601559	6.57	17.13	L06	0.925	1	BL	yes

<sup>‡</sup> Provenance of spectra: L06 - this paper, P06 - Papovich et al. (2006), SDSS - Sloan Digital Sky Survey data release 4.

\* Additional spectra obtained using COSMIC on the Palomar 200-inch, 2005, June 27-28

<sup>†</sup> Parts of a single galaxy

mid-infrared excess and is in the part of Figure 1 dominated by quiescent galaxies. This suggests that in some cases the signature of AGN activity in the mid-infrared can be overwhelmed by strong star formation activity, at least at  $z \lesssim 0.3$  where the PAH features can still contribute to the IRAC channel 4 flux. It may also indicate that much star formation activity (particularly any close to the nucleus) may be more obscured by dust than the narrow-line region of an AGN in the same galaxy. An AGN selection with the diagonal cut of the wedge raised by  $\approx +0.5$  in  $\lg(S_{8.0}/S_{5.8})$  would therefore increase the completeness of the AGN selection at low redshifts, though at the risk of reducing reliability.

## 6. The ratio of obscured to unobscured AGN

### 6.1. Redshift and luminosity distributions

Figure 9 shows the redshift histograms for our various classes of objects, compared to the redshift distribution of the sample as a whole.

Figure 10 shows the corresponding luminosity distributions of our objects. We calculate luminosities at a rest-wavelength of  $5\mu\text{m}$ . This region of the continuum is free from features, and can be calculated by interpolation between measurements over our full range of redshifts. The most heavily reddened AGN will, however, still be significantly extinguished at this wavelength, which is a possible bias in Figure 10.

As previously discussed, there are strong selection effects favoring the selection of low- $z$ , high luminosity AGN in our sample. Therefore we have made no attempt to investigate in detail the ratio of obscured to unobscured AGN as a function of redshift or luminosity to compare with, for example, the receding torus model of Lawrence (1991).

Overall, the breakdown into optical spectral types is as follows: 33% (25/77) normal type-1, 14% (11/77) reddened type-1, 44% (34/77) type-2 (including 2HZ), and 9% (7/11) starbursts and ambiguous starbursts/LINERs. Defining an obscured quasar as anything with  $E(B - V) \gtrsim 0.3$  in the rest frame and an AGN nature confirmed through optical emission lines or X-rays (the type-1Rs, type-2s, and the single X-ray detected starburst/LINER) we obtain a ratio of obscured to unobscured objects of 1.8:1. If we assume that

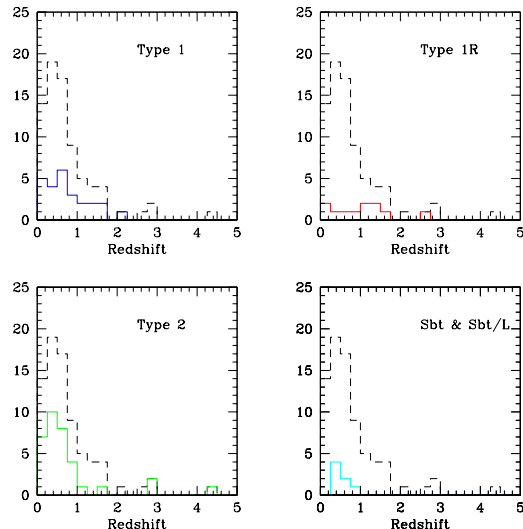


Fig. 9.— The redshift distribution for our different classes of object. The total distribution for the whole sample is shown as the dotted line on all the plots, and the solid line the distribution by type.

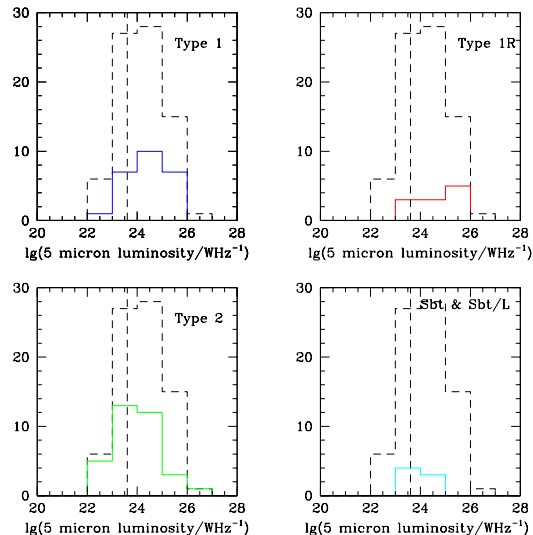


Fig. 10.— As Figure 6, but for rest-frame luminosity at  $5\mu\text{m}$ . The vertical dashed line is at the approximate division between Seyfert and quasar luminosities.

the other six starburst and starburst/LINER objects also contain obscured AGN this increases to 2.1:1.

The fraction of type-1Rs is higher than that found by Brown et al. (2006) in their  $24\mu\text{m}$  selected sample. Brown et al find 20% of their broad-line objects are classed as reddened type-1s, compared to a type-1R/(type-1+type-1R) fraction of 30% (14/46) in our sample. Our deeper spectroscopy limit ( $R \sim 23$  compared to  $R < 21.7$ ) is probably responsible for this difference. Two of our type-1R quasars have  $R < 21.7$ , and a third has  $R = 21.6$ , excluding these would reduce our type-1R fraction to 25%.

Before we can relate these ratios to an estimate of how much supermassive black hole growth is obscured, we need to bear in mind the intrinsic variations in quasar SEDs. Selection in the mid-infrared will inevitably mean our sample is biased in favor of objects whose intrinsic SEDs (before reddening of the quasar nucleus) are particularly bright in the mid-infrared, e.g. because of an unusually large dust covering factor. For type-1 and type-1R objects we have good evidence that this is not a large effect. Brown et al. (2006) find that the space density of their infrared-selected quasars is very similar to that of optically-selected samples, consistent with the small systematic variations seen in the quasar SEDs of Richards et al. (2006) and Hatziminaoglou et al. (2005) between optically-bright and infrared-bright quasars. Although our type-1 quasars at  $z > 1$  are redder in  $R$ -[8.0] color than the Richards et al. template color in Figure 5, most are close to the template, and several at  $z < 1$  are bluer. For the more heavily obscured objects there are two arguments that can be brought to bear. First, even in type-1 quasars about 40% of the UV emission is reprocessed by dust (Richards et al. 2006). Even if the obscured quasars have dust covering factors near unity, their dust emission would only increase by a factor  $\sim 2$  (and they would be significantly extinguished in the mid-infrared if that were the case, leading to their infrared luminosities being underestimated). Second, the majority of the obscured quasars possess luminous narrow emission lines, showing that a significant fraction of lines of sight from the nucleus are able to escape to ionize the narrow-line gas. Furthermore, in the case of radio-loud objects, where the radio lobe lu-

minosity provides an independent measure of the AGN luminosity, Haas et al. (2004b) find that radio-loud quasars and their type-2 equivalents, radio galaxies, show a statistically-identical ratio of radio to 10-1000 $\mu\text{m}$  infrared luminosity, indicating that the obscured population has a similar dust covering factor to the unobscured population, as expected from orientation-based Unified schemes (Antonucci 1993). We are thus confident that mid-infrared selection does not significantly bias an AGN sample towards objects with unusually high dust covering factors, and so we are fairly confident that our AGN sample is a fair proxy for one selected on the basis of bolometric flux. We can thus safely conclude that  $\sim 67\%$  of black hole growth in the redshift and luminosity range probed in this study is obscured by  $E(B - V) \gtrsim 0.3$ .

## 6.2. Comparison to other *Spitzer* selected samples

Mid-infrared selection of obscured AGN has been successfully performed by several other groups. Stern et al. (2005) use Hectospec data on the Böotes field to study AGN selected using a mid-infrared color cut similar to that in Figure 1, but with different axes. Plotting the objects of this paper onto the selection of Stern et al. we find that only a few obscured AGN found within our mid-infrared color criteria are missed by their color selection. They find an  $\approx 3 : 1$  ratio of obscured to unobscured AGN, somewhat higher than found in this study, which is  $\approx 2 : 1$ . However, as Richards et al. (2006) point out, their result relies on a power-law interpolation of the quasar SED between the mid-infrared and optical, which is not quite correct (see, e.g., the variation of  $R$ -[8.0] color in Figure 5), so their obscured AGN fraction may be overestimated. Alonso-Herrero et al. (2006) use another slightly different mid-infrared selection, based on the presence of a power-law mid-infrared SED, to find AGN in the Chandra Deep Field South. Due to this rather more complicated selection criterion it is hard to assess how many objects in the color-selected AGN samples would satisfy the selection criteria of Alonso-Herrero et al., but most of them are likely to, as our color criterion is very similar to a power-law selection. Their study complements the study of this paper very well, as their  $24\mu\text{m}$  fluxes range

from  $\approx 0.05 - 3\text{mJy}$  compared to our range of  $\approx 4.4 - 20\text{mJy}$ . Their median redshift of  $\sim 1.4$  (based mostly on photometric redshifts), compares with a median of 0.6 for the combined spectroscopic XFLS and SWIRE samples. Their objects are thus typically of similar, or only slightly lower luminosity to the objects in this study. The fact that they find a similar ratio of obscured to unobscured AGN of  $\approx 2 : 1$  (based on SED fitting) is therefore consistent with no strong dependence on this ratio on redshift in the range  $\sim 0.5 - 2$ .

Martínez-Sansigre et al. (2005,2006) use a different approach to selecting their obscured AGN. By searching for  $24\mu\text{m}$  sources with radio emission in excess of the radio-infrared correlation they are able to isolate obscured AGN irrespective of their mid-infrared SED shape. Although the properties of these radio-intermediate objects may be different from the predominately radio-quiet populations found from the mid-infrared color selection, the ratio of obscured to unobscured objects is similar, in the range 1-3:1.

In the X-ray, Alonso-Herrero et al. (2006), Donley et al. (2005) and Polletta et al. (2006) find a significant population (40-60%) of *Spitzer* selected AGN which are highly-obscured in the X-ray. In particular, many *Spitzer*-selected AGN in the samples of Alonso-Herrero et al. and Donley et al. are missing from even the  $\sim\text{Ms}$  exposures of the *Chandra* Deep Fields. 21 of the objects in our samples overlap *XMM-Newton* fields, we detect 14 of them in  $\sim 10 - 50\text{ks}$  exposures. Given the difference in flux limits at  $24\mu\text{m}$ , the relative X-ray depths are comparable, although the higher redshifts of the Alonso-Herrero et al. and Donley et al. samples should lead to these objects being more detectable at X-ray wavelengths due to the negative  $k$ -correction of an absorbed X-ray spectrum.

One final point of interest is that the three highest redshift objects in our sample are all obscured quasars. Although the statistics are small, the fact that these objects were found in spite of strong selection effects in favor of lower redshift objects is an indication that at very high redshifts ( $z \gtrsim 3$ ) obscured accretion may be even more common.

## 7. Conclusions

The results presented in this paper, taken together with studies of higher redshift objects se-

lected from mid-infrared deep fields and objects found using joint mid-infrared – radio selection show that a large population of luminous obscured AGN exist at  $z \gtrsim 0.3$ , including a significant population with bolometric luminosities above the Seyfert-quasar divide. We find that the obscured population dominates in number density over the unobscured one over a wide range in AGN luminosity, from Seyferts to luminous quasars. Comparison with Alonso-Herrero et al. (2006) suggests little variation in the obscured to unobscured ratio with redshift for AGN with strong mid-infrared emission.

Our results contrast with X-ray studies, which typically find that obscured AGN are confined to low redshifts ( $z \lesssim 1$ ) and luminosities below the Seyfert-quasar divide  $L_X \lesssim 10^{44}\text{ergs}^{-1}$  (e.g. Trump et al. 2006), suggesting that high luminosity and high redshift obscured quasars are missing from current X-ray based surveys, presumably due to limitations of areal coverage and depth. Although objects with columns  $N_H \sim 10^{23}\text{cm}^2$  can be found in deep X-ray surveys, locally  $\sim 50\%$  of AGN are Compton thick, with columns  $> N_H \sim 10^{24}\text{cm}^{-2}$ , and the equivalents of these objects at high redshifts would be very hard to find in the X-ray, even allowing for the positive  $k$ -correction. This has important implications for models of the X-ray background (e.g. Worseley et al. 2006). However, it is clear that all the techniques used to find obscured AGN are incomplete. Mid-infrared selection presumably fails for weak AGN, for highly obscured AGN, and at high redshifts. Our highest redshift objects are selected not on the basis of their hot dust emission, but on the basis of dust-reddened accretion disk emission, so we will inevitably miss the most obscured objects at  $z \gtrsim 3$ .

For most objects, classification of galaxy type (AGN or starburst) based on optical emission line ratios and classification based on mid-infrared IRAC color appear to agree fairly well. The mid-infrared criterion is seen to fail for  $z \lesssim 0.3$  AGN with strong PAH emission in the IRAC  $8.0\mu\text{m}$  band from an accompanying starburst. There are also some objects with AGN-like IRAC colors which lack the high-ionization emission line spectra of AGN. For most of these, their nature (AGN or starburst) remains to be resolved.

The discovery of a large population of ob-

scured AGN has important implications for accretion efficiency and black hole demographics. The mass density of black holes in the Universe today may be accurately estimated using the bulge-luminosity black hole mass relation, and the amount of accretion luminosity arising from unobscured accretion may be estimated from the optical quasar luminosity function (Soltan 1982). Recent estimates using this technique place the radiative efficiency of accretion close to that expected from a non-spinning (Schwarzschild) black hole (e.g. Yu & Tremaine 2002). However, if most accretion is actually hidden, to maintain the same mass density of black holes today in the face of more accretion activity requires a *higher* radiative efficiency, which can only be obtained from rapidly spinning Kerr black holes.

We would like to thank Alejo Martinez-Sansigre and Steve Rawlings for obtaining the WHT spectra, Michael Gregg for obtaining the Lick spectra, and the anonymous referee for a helpful report. The SWIRE team are thanked for producing and making available their *Spitzer* catalogs. Most of the optical data were obtained at the Hale Telescope, Palomar Observatory, as part of a continuing collaboration between the California Institute of Technology (CIT), the Jet Propulsion Laboratory (JPL) (operated by CIT for the National Aeronautics and Space Administration [NASA]), and Cornell University. ML and AP were visiting astronomers at the IRTF, which is operated by the University of Hawaii under Cooperative Agreement no. NCC 5-538 with the National Aeronautics and Space Administration, Science Mission Directorate, Planetary Astronomy Program. This paper is based on observations made with the *Spitzer Space Telescope* which is operated by JPL, CIT under a NASA contract. Support for this work was provided by NASA through JPL. Funding for the creation and distribution of the SDSS Archive has been provided by the Alfred P. Sloan Foundation, the Participating Institutions, NASA, the National Science Foundation, the U.S. Department of Energy, the Japanese Monbukagakusho, and the Max Planck Society. This research has made extensive use of the NASA/IPAC Extragalactic Database (NED) which is operated by JPL, CIT, under contract with NASA. Some of the data presented herein were obtained at the

W.M. Keck Observatory, which is operated as a scientific partnership among CIT, the University of California and NASA. The authors wish to recognize and acknowledge the very significant cultural role and reverence that the summit of Mauna Kea has always had within the indigenous Hawaiian community.

### A. Comparison of classifications with those of Papovich et al.

In an independent study, Papovich et al. (2006) obtained spectra of bright  $24\mu\text{m}$  XFLS sources with the Hectospec Fibre spectrograph on the MMT. Several of these objects are common to our XFLS AGN sample. Papovich et al. attempted to classify their objects using a semi-automated algorithm. For the most part, our classifications agree, and where we differ it is usually because the Papovich et al. “galaxy” classification generally includes narrow-line AGN (Table 6). There are, however, a few objects classed as broad line quasars or AGN for which there seems to be no evidence for broad lines in either our spectra or the Hectospec spectra. In one case, however, (SSTXFLS J171430.7+584225) the Hectospec spectrum does show weak broad  $\text{H}\beta$  and  $\text{MgII}2798$  emission, which appear very weak or absent in our Palomar/COSMIC spectrum. The Hectospec spectrum is of higher signal-to-noise than our spectrum, and the  $\text{H}\beta$  line falls close to the  $7600\text{\AA}$  atmospheric absorption feature (for which we do not attempt to correct), so it is most likely that we simply missed the weak broad  $\text{H}\beta$  line in this case. We have therefore reclassified this object as type-1R. One further discrepancy is in our classification of SSTSFLS J171454.4+584948, this object is classed at QSO/starburst by Papovich et al., but plots among the starbursts the BPT plot of Figure 4b, and has thus been classified as a starburst.

### B. Spectroscopy of the $8\mu\text{m}$ flux limited sample

Most of the objects in the  $8\mu\text{m}$  flux-limited sample of candidate obscured AGN of Lacy et al. (2004, 2005a) are also members of the XFLS sample of Table 3, however, a few have  $24\mu\text{m}$  fluxes below  $4.6\text{mJy}$  and are hence missing. For completeness we list their redshifts, where measured, and spectral types in Table 7 (see also Lacy et al. 2005).

Table 7: Non-SDSS objects in the XFLS sample with spectra in Papovich et al. (2006)

Name	$S_{24.0}/\text{mJy}^1$	Redshift	Class	Basis	P06 class*
SSTXFSL J171115.2+594906	9.4	0.587	Sbt		galaxy
SSTXFSL J171147.4+585839	4.8	0.800	2	[Nev]13	galaxy
SSTXFLS J171324.2+585549	4.9	0.609	2	[Nev]12	galaxy
SSTXFSL J171325.1+590531	9.5	0.126	2	BPT	QSO/AGN
SSTXFSL J171331.5+585804	5.9	0.435	Sbt/L		Galaxy
SSTXFSL J171335.1+584756	23.7	0.133	1R	FeII	QSO/BL
SSTXFSL J171430.7+584225	8.2	0.561	2	[Nev]20	QSO/BL
SSTSFSL J171454.4+584948	4.9	0.253	Sbt	BPT	Galaxy/starforming
SSTXFLS J171513.8+594638	5.0	0.248	1R	BL (radio-loud)	QSO/starburst
SSTXFSL J171530.7+600216	11.6	0.420	2	[Nev]26	QSO/BL
SSTXFSL J171650.6+595752	6.7	0.182	Sbt	BPT	galaxy/starburst
SSTXFSL J171708.6+591341	5.4	0.646	2	[Nev]37	QSO/BL
SSTXFSL J171839.6+593359	10.9	0.383	1	BL (radio loud)	QSO/BL
SSTXFSL J171913.5+584508	8.9	0.318	2	[Nev]12, BPT	QSO
SSTXFSL J172219.5+594506	7.8	0.271	2	BPT	QSO/AGN_BROAD
SSTXFSL J172228.1+601526	7.1	0.741	2	[Nev]	Galaxy/manual
SSTXFSL J172245.0+590328	4.7	0.797	2	[Nev]43	Galaxy

\* P06 class is the classification of the object in the MMT/Hectospec survey of Papovich et al. (2006), in the form class/subclass.

Table 8: Objects in the  $8\mu\text{m}$  selected sample of Lacy et al. 2004 not in the  $24\mu\text{m}$  flux-limited XFLS sample.

Name	$S_{8.0}$ (mJy)	$z$	Class	Basis
SSTXFSL J171106.8+590436	1.38	0.462	2?	[OIII]5007/[OIII]3727=3.8
SSTXFSL J171133.4+594906	1.91	?	1?	-
SSTXFSL J171421.3+602239	1.25	?	2/Sbt/L?	
SSTXFSL J171804.6+602705	1.05	0.43?	2/Sbt/L?	
SSTXFSL J171930.9+594751	1.44	0.358	2	[Nev]30
SSTXFSL J172253.9+582955	1.00	1.753*	1	BL
SSTXFSL J172458.3+591545	1.10	0.494	2?	[OIII]5007/[OIII]3727=1.8
SSTXFSL J172601.8+601100	1.43	1.12?	1R	single BL

\* spectrum from Papovich et al. (2006).

## REFERENCES

- Alonso-Herrero, A. et al. 2006, *ApJ*, 640, 167
- Antonucci, R. 1993, *ARA&A*, 31, 473
- Baldwin, J.A. Phillips, M.M. & Terlevich, R. 1981, *PASP*, 93, 5
- Barmby, P. et al. 2006, *ApJ* in press (astro-ph/0512618)
- Becker, R.H. et al. 2001, *ApJS*, 135, 227
- Brand, K. et al. 2006, *ApJ*, in press (astro-ph/0602198)
- Brown, M.J. et al. 2006, *ApJ*, 638, 88
- Caccianiga, A., et al. 2004, *A&A*, 416, 901
- Chiappetti, L. et al. 2005, *A&A*, 439, 413
- Comastri, A., Setti, G., Zamorani, G. & Hasinger, G. 1995, *A&A*, 296, 1
- Comastri, A. et al. 2002, *ApJ*, 571, 771
- Condon, J.J., Cotton, W.D., Yin, Q.F., Shupe, D.L., Storrie-Lombardi, L.J., Helou, G., Soifer, B.T. & Werner, M.W. 2003, *AJ*, 125, 2411 G.P. 2003, *ApJ*, 584, L57
- Cutri, R.M., Nelson, B.O., Kirkpatrick, J.D., Huchra, J.P. & Smith, P.S. 2001, in *ASP Conf. Ser. 232, The New Era of Wide Field Astronomy*, ed. R. Clowes, A. Adamson, & G. Bromage (San Francisco: ASP), 78
- Donley, J.L., Rieke, G.H., Rigby J.R. & P'erez-Gonzales, P.G. 2005, *ApJ*, 634, 169
- Eckart, M.E. et al. 2006, *ApJS*, 165, 19
- Fadda, D., Jannuzi, B., Ford, A. & Storrie-Lombardi, L.J. 2004, *AJ*, 128, 1
- Fadda, D. et al. 2006, *AJ*, 131, 2859
- Glikman, E., Gregg, M.D., Lacy, M., Helfand, D.J., Becker, R.H. & White, R.L. 2004, *ApJ*, 607, 60
- Grimes, J.P. Kriss, G.A. & Espey, B.R. 1999, *ApJ*, 526, 130
- Haas, M. et al. 2004a, *A&A*, 219, L49
- Haas, M. et al. 2004b, *A&A*, 424, 531
- Hatziminaoglou, E. 2005, *AJ*, 129, 1198
- Kauffmann, G. et al. 2003, *MNRAS*, 346, 1055
- Kewley, L.J., Groves, B., Kauffmann, G. & Heckman, T. 2006, *MNRAS*, submitted (astro-ph/0605681)
- Lonsdale, C.J. et al. 2003, *PASP*, 115, 897
- Lacy, M. et al. 2004, *ApJS*, 154, 166
- Lacy, M. et al. 2005a, *MmSAI*, 76, 154
- Lacy, M. et al. 2005b, *ApJS*, 161, 41
- Leipski, C. et al. 2005, *A&A*, 440, L5
- Lawrence, A. 1991, *MNRAS*, 252, 586
- Martínez-Sansigre, A. et al. 2005, *Nat*, 436, 666
- Martínez-Sansigre, A. et al. 2006, *MNRAS*, 370, 1479
- Mason, R.E. et al. 2006, *ApJ*, 640, 612
- Meisenheimer, K., Haas, M., Müller, S.A.H., Chini, R., Klaas, U. & Lemke, D. 2001, *A&A*, 372, 719
- Michel, L., Herent, O. Motch, C., Pye, J. & Watson, M.G. 2004, in *Astronomical Data Analysis Software and Systems XIII*, Oschenbein, M., Allen, M. & Egret, D. eds, *ASP Conf. Ser.* 314, p. 570
- Moran, E.C., Filippenko, A.V. & Chornock, R. 2002, *ApJ*, 579, 71
- Petric, A. et al. 2006, in preparation
- Norman, C. 2002, *ApJ*, 571, 218
- Ogle, P., Whysong, D. & Antonucci, R. 2006, *ApJ*, submitted (astro-ph/0601485)
- Papovich, C. et al. 2006, *AJ*, 132, 231
- Pei, Y.C. 1992, *ApJ*, 395, 130
- Polletta, M. et al. 2006, *ApJ*, 642, 673
- Rayner, J.T. et al. 2003, *PASP*, 115, 362
- Richards, G.T. et al. 2006, *ApJS*, submitted (astro-ph/0601558)

- Rigby, J.R., Rieke, G.H., Donley, J.L., Alonso-Herrero, A. & Pérez-González, P.G. 2006, *ApJ*, 645, 115
- Siana, B. et al. 2006, to appear in “Infrared Diagnostics of Galaxy Evolution”, ed. R. Chary (astro-ph/0604373)
- Sajina, A., Lacy, M. & Scott, D. 2005, *ApJ*, 621, 256
- Sharp, R. G., Sabbey, C. N., Vivas, A. K., Oemler, A., McMahon, R. G., Hodgkin, S. T., & Coppi, P. S. 2002, *MNRAS*, 337, 1153 & Yang, T. 2003, *ApJ*, 596, L23
- Soltan, A. 1982, *MNRAS*, 200, 115
- Spinoglio, L., Malkan, M.A., Rush, B., Carrasco, L. & Recillas-Cruz, E. 1995, *ApJ*, 453, 616
- Treister, E. et al. 2004, *ApJ*, 616, 123
- Trump, J.R. et al. 2006, *ApJS*, in press (astro-ph/0606016)
- van Ojik, R., Röttgering, H.J.A., Miley, G.K., Bremer, M.N., Maccetto, F. & Chambers, K.C. 1994, *A&A*, 289, 54
- Watson, M.G., et al. 2004, AAS/High Energy Astrophysics Division, 8.3701
- Weedman, D. Le Floch, E., Higdon, S.J.U., Higdon, J.L. & Houck, J.R. 2006, *ApJ*, 638, 613
- Worsley, M.A. et al. 2005, *MNRAS*, 357, 1281
- Yu, Q. & Tremaine, S. 2002, *MNRAS*, 335, 965
- Yuan, F. & Narayan, R. 2004, *ApJ*, 612, 724
- Zakamska, N.L. et al. 2003, *AJ*, 126, 2125